NASA/CR—2004–213227

Analysis of CRRES PHA Data for Low-Energy-Deposition Events

P.J. McNulty
Clemson University, Clemson, South Carolina

Prepared for Marshall Space Flight Center
under H-Order 32495D
and sponsored by
The Space Environments and Effects Program
managed at the Marshall Space Flight Center

June 2004

The NASA STI Program Office…in Profile

Since its founding, NASA has been dedicated to the advancement of aeronautics and space science. The NASA Scientific and Technical Information (STI) Program Office plays a key part in helping NASA maintain this important role.

The NASA STI Program Office is operated by Langley Research Center, the lead center for NASA's scientific and technical information. The NASA STI Program Office provides access to the NASA STI Database, the largest collection of aeronautical and space science STI in the world. The Program Office is also NASA's institutional mechanism for disseminating the results of its research and development activities. These results are published by NASA in the NASA STI Report Series, which includes the following report types:

- TECHNICAL PUBLICATION. Reports of completed research or a major significant phase of research that present the results of NASA programs and include extensive data or theoretical analysis. Includes compilations of significant scientific and technical data and information deemed to be of continuing reference value. NASA's counterpart of peer-reviewed formal professional papers but has less stringent limitations on manuscript length and extent of graphic presentations.

- TECHNICAL MEMORANDUM. Scientific and technical findings that are preliminary or of specialized interest, e.g., quick release reports, working papers, and bibliographies that contain minimal annotation. Does not contain extensive analysis.

- CONTRACTOR REPORT. Scientific and technical findings by NASA-sponsored contractors and grantees.

- CONFERENCE PUBLICATION. Collected papers from scientific and technical conferences, symposia, seminars, or other meetings sponsored or cosponsored by NASA.

- SPECIAL PUBLICATION. Scientific, technical, or historical information from NASA programs, projects, and mission, often concerned with subjects having substantial public interest.

- TECHNICAL TRANSLATION. English-language translations of foreign scientific and technical material pertinent to NASA's mission.

Specialized services that complement the STI Program Office's diverse offerings include creating custom thesauri, building customized databases, organizing and publishing research results…even providing videos.

For more information about the NASA STI Program Office, see the following:

- Access the NASA STI Program Home Page at ***http://www.sti.nasa.gov***

- E-mail your question via the Internet to help@sti.nasa.gov

- Fax your question to the NASA Access Help Desk at (301) 621–0134

- Telephone the NASA Access Help Desk at (301) 621–0390

- Write to:
  NASA Access Help Desk
  NASA Center for AeroSpace Information
  7121 Standard Drive
  Hanover, MD 21076–1320
  (301)621–0390

NASA/CR—2004–213227

Analysis of CRRES PHA Data for Low-Energy-Deposition Events

P.J. McNulty
Clemson University, Clemson, South Carolina

Prepared for Marshall Space Flight Center
under H-Order 32495D
and sponsored by
The Space Environments and Effects Program
managed at the Marshall Space Flight Center

National Aeronautics and
Space Administration

Marshall Space Flight Center • MSFC, Alabama 35812

June 2004

Acknowledgments

This effort was accomplished with resources provided by NASA's Living With a Star (LWS) Space Environment Testbeds (SET) Program.

Available from:

NASA Center for AeroSpace Information
7121 Standard Drive
Hanover, MD 21076–1320
(301) 621–0390

National Technical Information Service
5285 Port Royal Road
Springfield, VA 22161
(703) 487–4650

TABLE OF CONTENTS

LIST OF FIGURES

LIST OF FIGURES (Continued)

CONTRACTOR REPORT

ANALYSIS OF CRRES PHA DATA FOR LOW-ENERGY-DEPOSITION EVENTS

1. BACKGROUND

The objective of this work was to analyze the low-energy deposition Pulse Height Analyzer (PHA) data from the Combined Release and Radiation Effects Satellite (CRRES). The high-energy-deposition data had been analyzed previously (1,2) and been shown to be in agreement with spallation reactions predicted by the Clemson University Proton Interactions in Devices (CUPID) simulation model (3) and existing environmental and orbit positioning models (AP-8 with USAF B-L coordinates). With older technology devices, only high-energy depositions were capable of generating a threshold amount of charge within the sensitive volume and thus force the device to switch logic states. However, modern devices have much lower thresholds (critical charges), and there is experimental data, which suggest that this data requires additional mechanisms to explain the rates at which single event upsets (SEUs) now occur. This is particularly true when the devices are sensitive to low-energy neutrons such as those coming from a radioactive source (See Appendix A). These neutrons have such low energy that spallation reactions are not expected to be important but elastic reactions and direct ionization from the primary can be important. Also, in space a small fraction of the trapped protons are incident with sufficient kinetic energy to generate pions during the interaction. Since the pions are neutral in charge or leave the detector with minimum linear energy transfer (LET), this should significantly change the amount of energy deposited locally within the sensitive volume of the detector.

The scope of this project was to develop and improve the CUPID model by increasing its range to lower incident particle energies, and to expand the modeling to include contributions from elastic interactions. Before making changes, it was necessary to identify experimental data suitable for benchmarking the codes. Then we could apply the models to the CRRES PHA data. It was also planned to test the model against available low-energy proton or neutron SEU data obtained with mono-energetic beams.

2. WORK DONE UNDER CONTRACT

1ST Quarter:

- Selected benchmark data set (4) from a large Li-drifted Si detector exposed by the Johns Hopkins APL group to neutrons at Los Alamos neutron facility (5). The energy of each individual neutron was determined by time of flight techniques. Data was available with incident energies ranging from 20 to 600 MeV (4).

- Simulations with the old version of CUPID were carried out to compare with the experimental data, and the deficiencies in the original model determined. At incident energies above the threshold for pion production, the theory were significantly overestimated the number of large-energy-deposition events. This deviation is evident in the comparison of the original CUPID with data obtained from a 2 cm^2 area detector with a thickness of 5mm exposed to neutrons incident at 200 MeV shown in Fig. 1. This deviation is not evident at incident energies below the pion threshold as illustrated for neutrons incident at 50 and 100 MeV. This deviation at large energy depositions increases with incident neutron energy as shown in Fig. 2. This is presumably due to the fact that CUPID does not include the effects of pion production, and any pion produced removes at least the amount of energy equivalent to its mass from what can be deposited locally in the detector. Also, the theory underestimated the number of low-energy-deposition events due to two reasons: 1) Events due to elastic scattering were not included and 2) the transformation of high-energy events to low-energy events due to pion production was not included. The close agreement between the proton and neutron simulations forms the basis of the use of neutrons to calibrate the models for predictions for protons in space.

- CUPID greatly over-predicted the experimental data over all energy depositions for incident particle energies below 50 MeV. This is illustrated in Fig. 3 for neutrons incident at 20 MeV. CUPID assumes that the incident particle interacts with the individual nucleons. However, at low energies the DeBroglie wavelength of the neutron is larger than the entire nucleus, and the total cross section is reduced to the neutron-nucleus cross section. The resulting large difference between experiment and theory, almost 2 orders of magnitude, is shown for neutrons incident at 20 MeV in the figure.

2nd Quarter:

- Prepared paper for presentation as a late-news paper at the Radiation Effects in Components and Systems (RADECS) conference. This paper describes the evidence for contributions from elastic interactions to SEU events at low incident energies but not at high energies for one device and for another device at low incident energies and at high energies when the critical charge is reduced. The excellent agreement at large incident energies and the disagreement at low incident energies are illustrated in Figs. 4 through 7. A copy of the paper is presented in Appendix A.

- Extended the comparison with experiment to incident energies up to 600 MeV. We found that most pion producing events generate low-energy depositions rather than high-energy depositions. Therefore, pion production introduces a significant contribution to the low-energy deposition portion of the spectrum as well as decreasing the high-energy-deposition events. Sample comparisons are shown in Figs. 8 and 9 as line plots to make the deviations easier to distinguish.

3rd Quarter

- Prepared a summary for the Nuclear and Space Radiation Effects Conference (NSREC) on the effect of pion production on the energy-deposition events in large sensitive volumes. This paper presented preliminary modifications to the CUPID model and compared predictions of the modified model with experimental data. The results of the comparison are summarized in Fig. 10 for four incident neutron energies above the threshold for pion production. In all four cases, the fits between theory and experiment are excellent.

4th Quarter:

- Prepared a manuscript describing the impact of pion production on energy-deposition events in large volumes of Silicon. A copy of the paper is presented in Appendix B.
- Completed the preliminary version of the pion production model for energy deposition events.
- Completed the algorithm for calculating the number of events generated by elastic scattering.
- Performed CUPID calculations for the UV100 detector that flew on CRRES for protons incident with energies from 30 to 600 MeV.
- Completed a comparison of theory and experiment.

3. TECHNICAL DISCUSSION

The CUPID codes needed three updates in order to provide good fits to experimental energy-deposition spectra over the entire range of energy depositions and over the entire range of incident energies. First, the codes should include the contribution from elastic nuclear scattering. Second, they should predict the correct total number of events even at low energies. Finally, the calculations should include the contributions from pion production. A two-prong approach was adopted. In this work, the detector of interest was a large volume detector which meant that the energy deposition by secondary particles form a major contribution to the measured energy-deposition spectra. In general, SEU-sensitive devices have sensitive volumes with microscopic dimensions, and the energy deposition by the recoil dominates. A graduate student is currently completing a thorough modification of the codes in order to take all three effects into account on an event-by-event basis in the codes in a manner that can be used on small microvolumes. This study concentrates on predictions for macroscopic volumes such as the CRRES UV100 detector.

Pion Production

The kinematics of elastic and quasi-elastic interactions between the incident nucleus and the target nucleons within the nucleus are determined in the CUPID codes (3,6) by the trajectory of the incident particle. For an elastic collision, the value of the impact parameter uniquely determines the amount of energy transferred to the target nucleon during the collision (7). When the collision occurs inside a nucleus, both the incident and scattered particles may interact with other nucleons before leaving the nucleus. The energy transferred in the primary collision is uniquely determined by the impact parameter, the perpendicular distance between the trajectory of the incident particle and a parallel trajectory that passes through the center of the target nucleon. Subsequent collisions within the nucleus result in the emission of secondary particles either immediately or during the subsequent “evaporation” of the residual nucleus.

If the impact parameter is small enough that more than 140 MeV would be transferred in the center of momentum frame, then there is sufficient energy transfer to produce a pion. If a pion is produced, it will almost certainly escape from a light nucleus like Silicon taking with it the energy equivalent of its rest mass (140 MeV) from the energy available for localized energy deposition within the detector. The production of two pions would lower the localized energy deposition by 280 MeV, and so on. In this preliminary version of the modified code, each time more than 140 MeV was to be transferred in the primary collision, the energy transferred to the target nucleon was reduced by 140 MeV and the interaction was allowed to continue. The energy deposition within the sensitive volume was then calculated in the normal manner. The fraction of events in which a pion is produced is plotted in Fig. 11 versus the kinetic energy of the incident particle.

Clearly, the fraction of events in which a pion is produced is small, but pions are entirely generated in potentially high energy-deposition events and the reduction of the localized energy deposition in these events has a dramatic impact on the energy-deposition spectra as can be seen in Fig. 10. The inclusion of pion production removes the discrepancy between theory and experiment at large energy depositions. It also increases the number of low energy-deposition events.

Elastic Scattering

The energy deposition spectra measured at low incident energies are dominated by elastic scattering events, especially at low energy depositions. The cross section for elastic scattering has a complicated dependence on the angle of scattering (7). However, all of the energy carried by the recoiling Silicon nucleus remains within the sensitive volume for volumes as large as the Li-drifted Silicon detector (4) or the UV100 flown on CRRES (1). Moreover, examination of all the neutron data sets shows that the elastic contribution to the energy deposition spectra falls off linearly with the energy deposited. Furthermore, for incident particle energies below 80 MeV, the elastic scattering cross section is approximately equal to the spallation-reaction cross section. Finally, the upper limit to the recoil energy established by kinematics is easily calculated (7). This provides us with a simple method for including the contribution for elastic scattering in the energy range between 30 and 80 MeV. At the lowest energy deposition, the integral elastic cross section is taken to be equal to the spallation reaction cross section calculated by CUPID. At the energy deposition equal to the largest elastic recoil set by kinematics, the integral elastic cross section is zero. A linear dependence on the energy deposition (recoil energy) is assumed for all intermediate values of the energy deposition. The total integral cross section is then the sum of the elastic and spallation cross sections. The contribution from elastic scattering is best seen on a linear scale, and a comparison of theory and experiment is shown for incident energies between 40 and 70 MeV in Fig. 12. The agreement is excellent for incident energies greater than and equal to 40 MeV. At 30 MeV the total energy deposition cross sections predicted by theory is about a factor of 4 greater than the experiment. This is shown in Fig. 13.

For incident energies above 100 MeV, the physics of the interactions is more complicated. Since the incident particle interacts with the individual nucleons inside the nucleus, the relationship between the elastic and spallation cross sections was less obvious. At incident energies above 100 MeV, the elastic cross section was taken to be the difference between the total cross section measured with Los Alamos National Laboratories (LANL) neutrons and the value given by CUPID simulations. Again, the integral elastic cross section was assumed to fall off linearly with energy deposition. This algorithm provided very good agreement with the measured spectra as can be seen in the comparisons shown in Figs. 13 and 14.

The measured total cross sections are plotted versus the kinetic energy of the incident neutron in Fig. 15. The resonance at the lower incident energies is clearly evident. The calculated total cross sections are in sufficient agreement with experiment for incident

energies above 30 MeV that no correction to the theoretical values was used in what follows. At 30 MeV, the theoretical cross section had to be reduced by a factor of four to bring it into agreement with theory. This correction is used in what follows.

Calculations for the CRRES UV100

Cupid simulations were carried out for the UV100 detector. The detector had a sensitive volume with a cross sectional area of 5 mm^2 and a thickness of 26 μm. The simulation codes included corrections for pion production but not elastic scattering. Since the elastic recoils are so short, they were assumed to remain within the detector over their entire range, and the elastic cross sections obtained for the larger Li-drifted Silicon detector were scaled for the UV100 by multiplying by the ratio of the volumes. Calculations were carried out for incident energies of 30, 40, 50, 60, 70, 80, 90, 120, 150, 180, 210, 240, 270, 300, 330, 360, 390, 420, 450, 480, 510, 540, 570, and 600 MeV, a total of 24 source terms. The number of events in the UV100 in which energy ED_j was deposited, COUNTS (ED_j) is given by:

$$\text{COUNTS } (ED_j) = \Sigma_i \, [\, F(E_I) \, \text{CUPID}_I \, (ED_j)]$$

where E_I represents each of the 24 incident energies for which the CUPID simulations have been calculated and CUPID_I (ED_j) is the total differential cross section for generating the events in which energy ED_j is deposited. The cross sections were calculated for an incident particle with kinetic energy E_i. The term $F(E_I)$ represents the fluence of protons with energy E_i. The experimental CRRES data for orbits 4 through 584 were substituted for each value of COUNTS (ED_j) and the equation was best fitted to find the optimum values of the flux $F(E_I)$. The values of the fluence obtained are plotted in Fig. 16.

Using the best-fit values for the fluence, the predicted integral energy-deposition spectrum was calculated and compared to the spectrum measured with the UV100 detector on CRRES during orbits 4 through 584. This was carried out as a check that our best-fit analysis was in fact converging on a valid solution. The comparison is shown in Fig. 17 where it is seen that the agreement is excellent over the entire range of energy depositions. The predictions by Reed (1,2) of the same spectrum using the original version of CUPID and the fluence values obtained from AP8 and the USAF B-L coordinates for the satellite are also shown. Comparing Reed's calculations with those of the present study highlights where the elastic scattering contributes at low energy depositions and pion production reduces the tail of the distribution at high-energy depositions.

Since the original best fit analysis was carried out using the integral form of the data, a more interesting comparison would be with the differential form of the spectrum. This comparison is shown in Fig. 18 for the differential energy-deposition spectra. Again, the fit is excellent. The cosmic-ray events at very large energy depositions are clearly evident and were removed from the integral comparison above.

4. SUMMARY AND CONCLUSIONS

Correction algorithms were devised for the CUPID codes which included the contributions of elastic scattering and pion production. The results were compared to the measurements of Kinnison et al. (4) of energy-deposition spectra measured with a Li-drifted Silicon detector with a cross sectional area of 2 cm^2 and a thickness of 5 mm. The agreement was very good for both the contributions of pion production to the large energy depositions and that of elastic scattering at low energy depositions. The simulation codes were then used to calculate the spectra for the UV100 detector (area = 50 mm^2, thickness = 26μm). The corrections for elastic scattering were scaled between the detectors by the ratio of the volumes. The results of these simulations were compared to the measurements from orbits 4 through 584 on the CRRES satellite in order to determine the fluence that would provide the best fit to the data. The measured fluence is in reasonably good agreement with the predictions of the NASA model.

There is evidence for significant contributions to the spectrum measured by the UV100 from both elastic scattering at low energy depositions and pion production at high energy depositions. Moreover, there are a small number of large pulses in the data from direct traversals of the detector by heavy cosmic-ray ions. Most of these could be removed by designing the sensitive volume of the detector as an array of p-n micro-junctions rather than a single large junction (8).

5. REFERENCES

1. R.A. Reed, P.J. McNulty, W.J. Beauvais, W.G. Abdel-Kader, E.G. Stassinopoulos, and J.C.L. Barth, "A Simple Algorithm for Predicting proton SEE Rates in Space Compared to the Rates in Space Measured on the CRRES Satellite", IEEE Trans. Nucl. Sci. 41, 2389-2395 (1994).
2. R.A. Reed, "Predicting Proton-Induced Single Event Upset Rates", Ph.D. dissertation submitted to Clemson University 1994.
3. G. E. Farrell, P. J. McNulty, and W. G. Abdel-Kader, "Microdosimetric Analysis of Proton-Induced Reactions in Silicon and Gallium Arsenide", IEEE Trans. Nucl. Sci. NS-31, 1073-1077 (1984).
4. J.D. Kinnison, R.H. Maurer, D.R. Roth, and R.C. Haight, "High-Energy Neutron Spectroscopy with Thick Silicon Detectors" Rad. Res. 159, 154-160 (2003).
5. P.W. Lisowski, C.D. Bowman, G.J. Russell, and S.A. Wender, "The Los Alamos National Laboratory Spallation neutron Sources," Nucl. Sci. Eng., 106, 208 (1990).
6. G.E. Farrell, "Energy Deposition by Nuclear Interactions in Microscopic Volumes," Ph.D. dissertation submitted to Clarkson University 1983.
7. E. Segre, "Nuclei and Particles", (W. A. Benjamin Inc., New York City, 1965).
8. D.R. Roth, P.J. McNulty, W.J. Beauvais, R.A. Reed, and E.G. Stassinopoulos, "Solid-State Microdosimeter for Radiation Monitoring in Spacecraft and Avionics", IEEE Trans. Nucl. Sci. 41, 2118-2124 (1994).

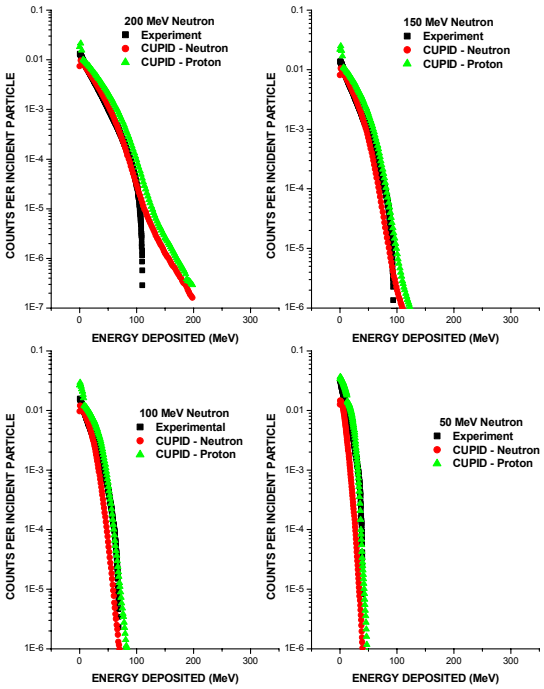

Fig. 1 Number of events in which at least energy E is deposited in a room temperature Si Li-drifted detector plotted versus E for incident neutron energies of 50, 100, 150 and 200 MeV. The detector has a cross sectional area of 2 cm^2 and a thickness of 0.5 mm.

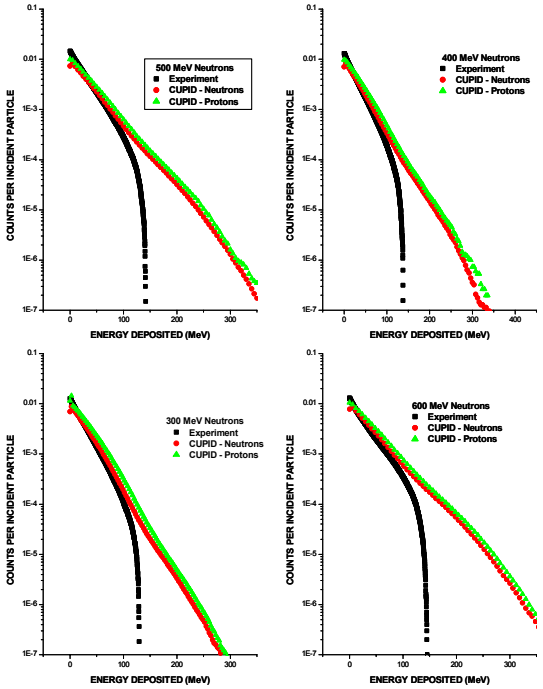

Fig. 2 Count rate per incident neutron for events in which at least energy E is deposited within a Si Li-drifted detector for incident energies of 300, 400, 500, and 600 MeV. The cross sectional area of the detector is 2 cm^2 and the thickness is 0.5 mm.

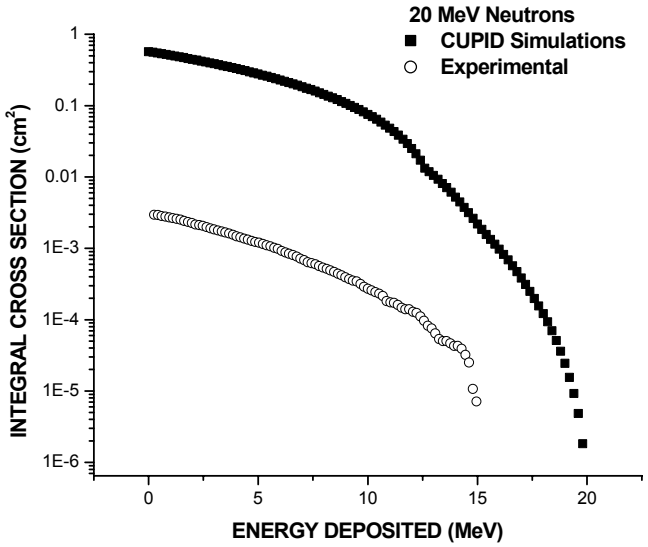

Fig. 3. Cross section for spallation reactions which deposit at least energy E within a Si detector with cross sectional area 64 mm^2 and thickness of 5 mm. The cross sections are for interactions generated by neutrons incident with 20 MeV kinetic energy.

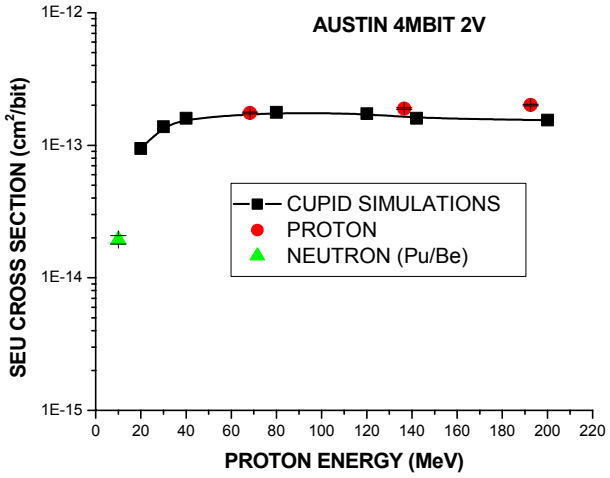

Fig. 4 SEU cross section versus incident particle energy for Austin 4 Mbit SRAMs exposed to high-energy protons and low-energy neutrons from a Pu/Be radioactive source while biased at 2 V. Excellent agreement except for the neutron data because no spallation SEU events are predicted.

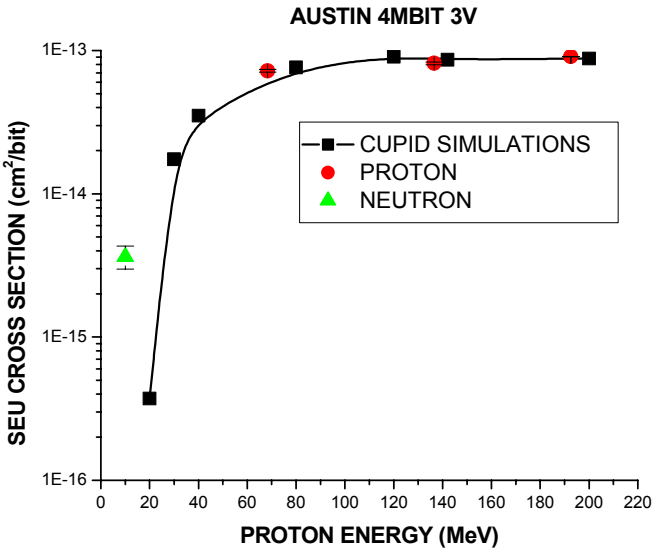

Fig. 5 SEU cross section versus incident particle energy for 4 Mbit SRAM exposed to high-energy protons and low-energy neutrons while biased at 3 V. Again, there is agreement at high energies but not at low energies.

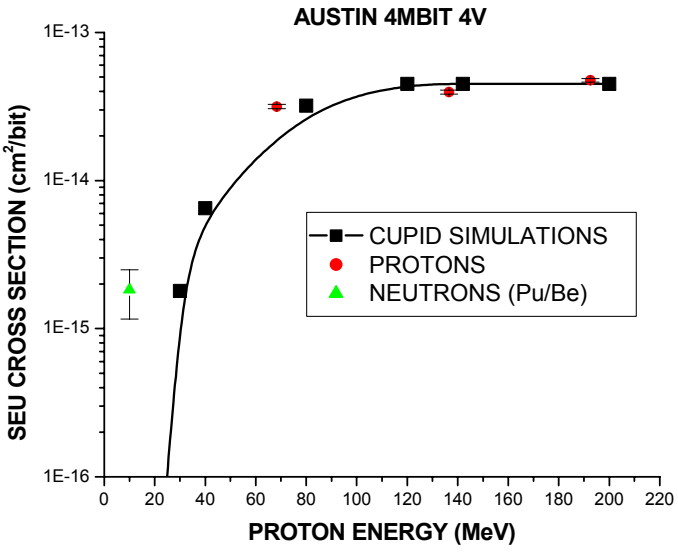

Fig. 6 SEU cross section versus incident particle energy for a 4 Mbit SRAM exposed to high-energy protons and low-energy neutrons while biased at 4 V.

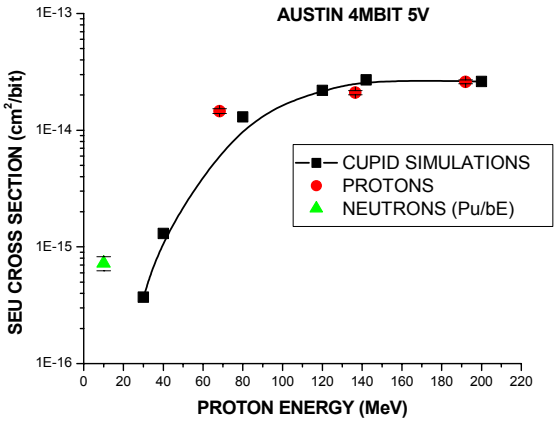

Fig. 7 SEU cross section versus incident particle energy for an Austin 4 Mbit SRAM exposed to high-energy protons and low-energy neutrons while biased at 5 V.

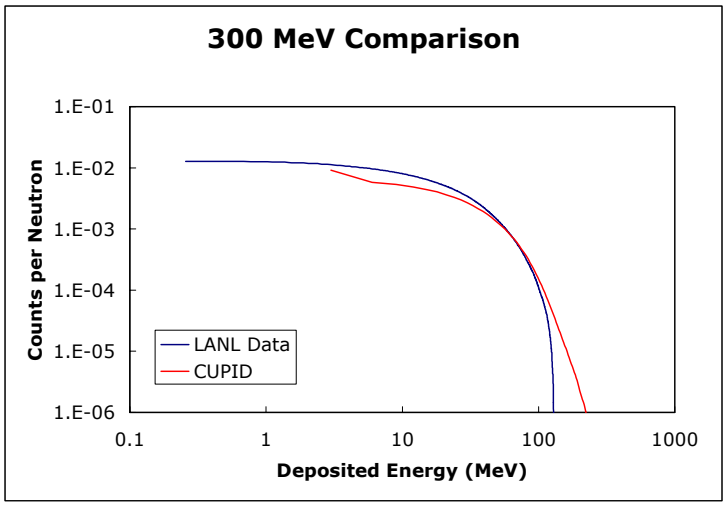

Fig. 8 Comparison of CUPID with experimental data obtained by the JHUAPL group for neutrons incident at 300 MeV.

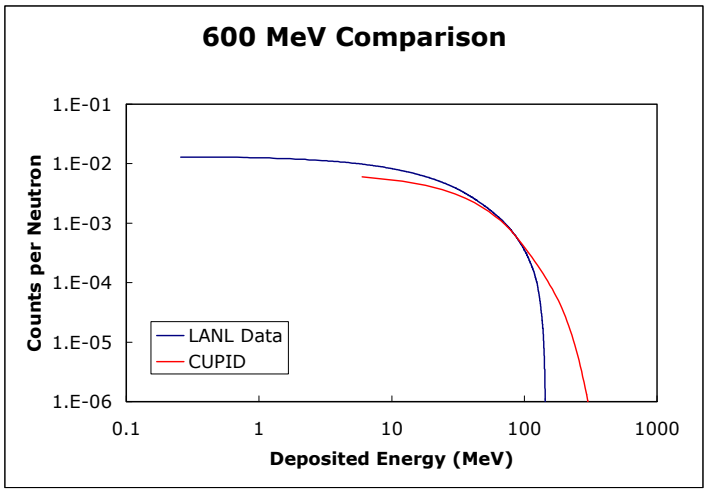

Fig. 9 Comparison of CUPID simulations for 600 MeV incident neutrons with experimental data from the JHUAPL group. The deviations at this energy represent about 10% of the data.

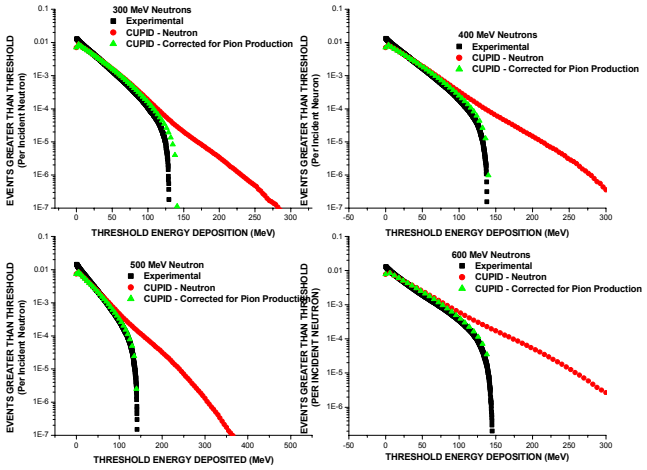

Fig. 10 Comparison of CUPID with and without corrections for pion production with experimental data for incident neutron energies of 300, 400, 500, and 600 MeV.

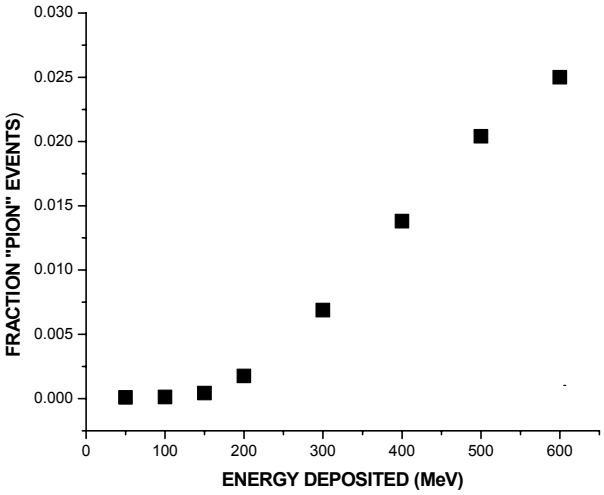

Fig. 11 Fraction of all energy-deposition events in which a pion is generated as a function of the kinetic energy of the incident particle.

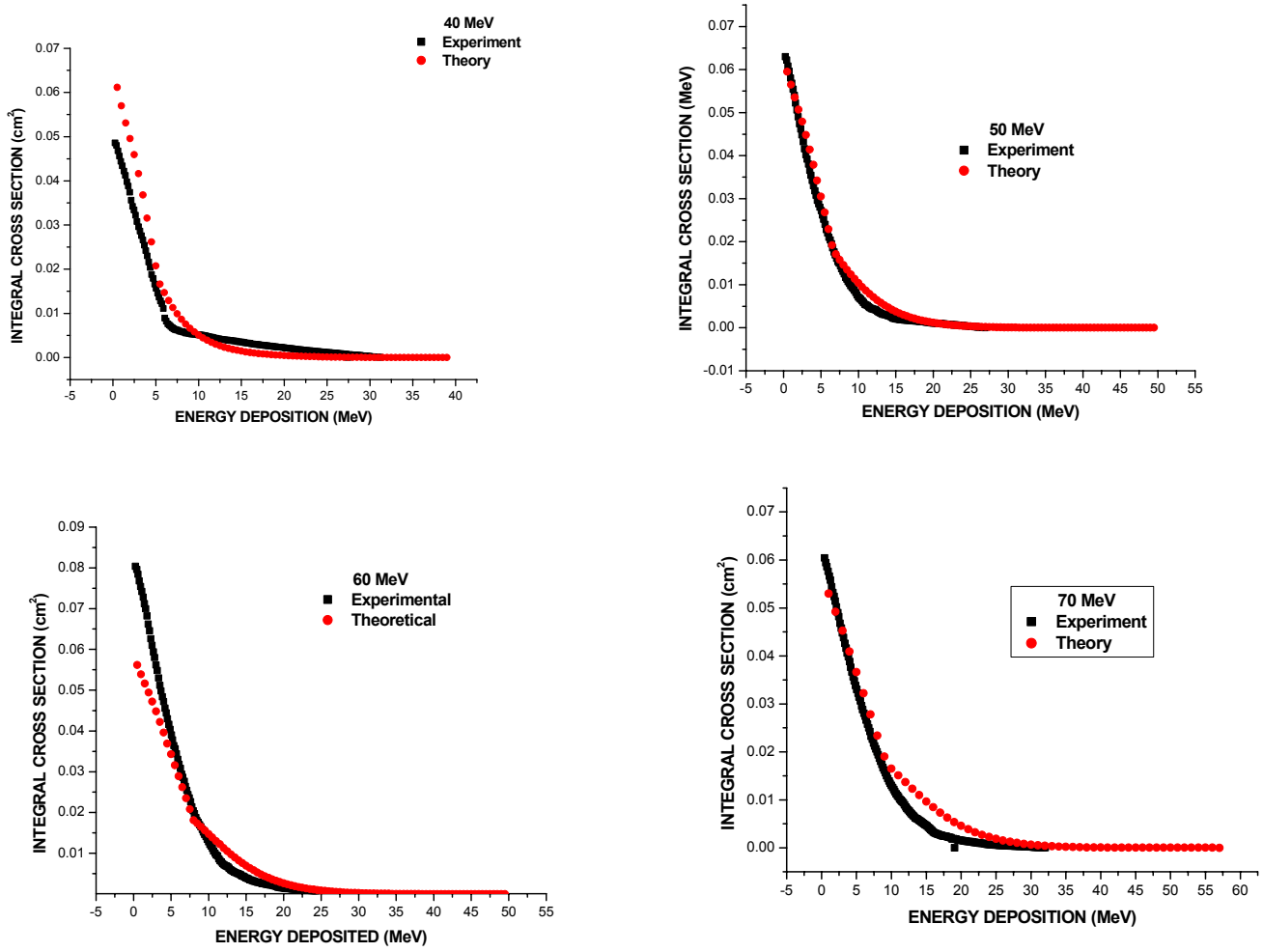

Fig. 12 Number of events in which at least energy E is deposited in a Li-drifted Silicon detector with a cross sectional area of 2 cm^2 and a thickness of 5 mm plotted versus the deposited energy E. The incident neutron energies are 40, 50, 60, and 70 MeV.

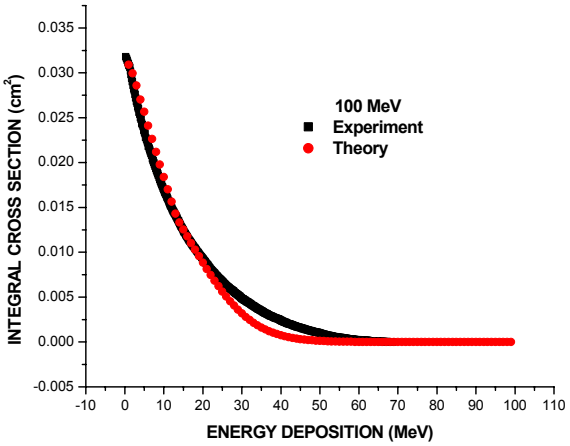

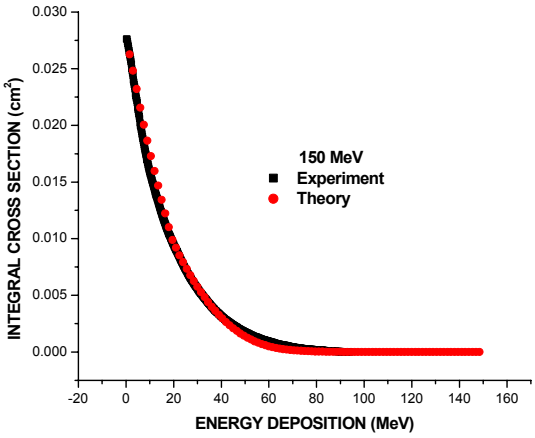

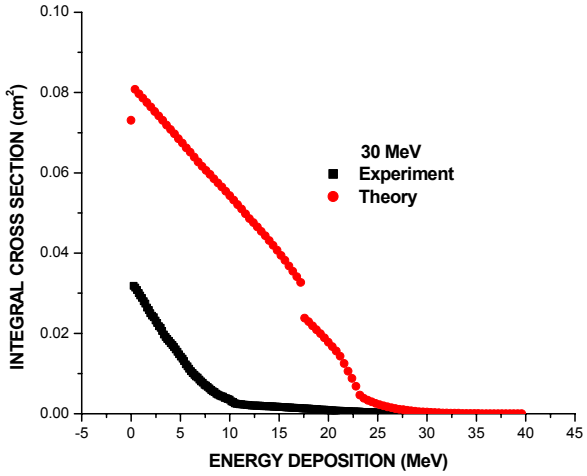

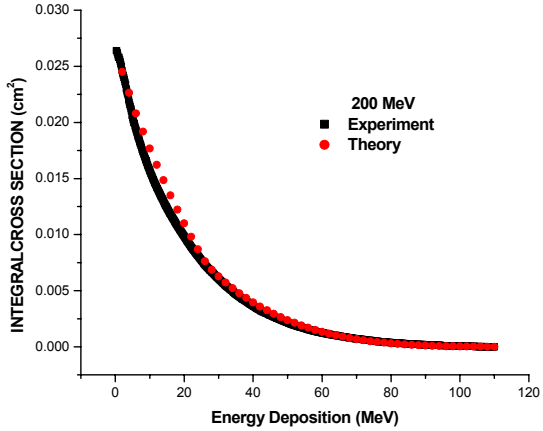

Fig. 13 Number of events in which at least energy E is deposited in the detector plotted versus E. The incident neutron energies are 100, 150, 200, and 30 MeV.

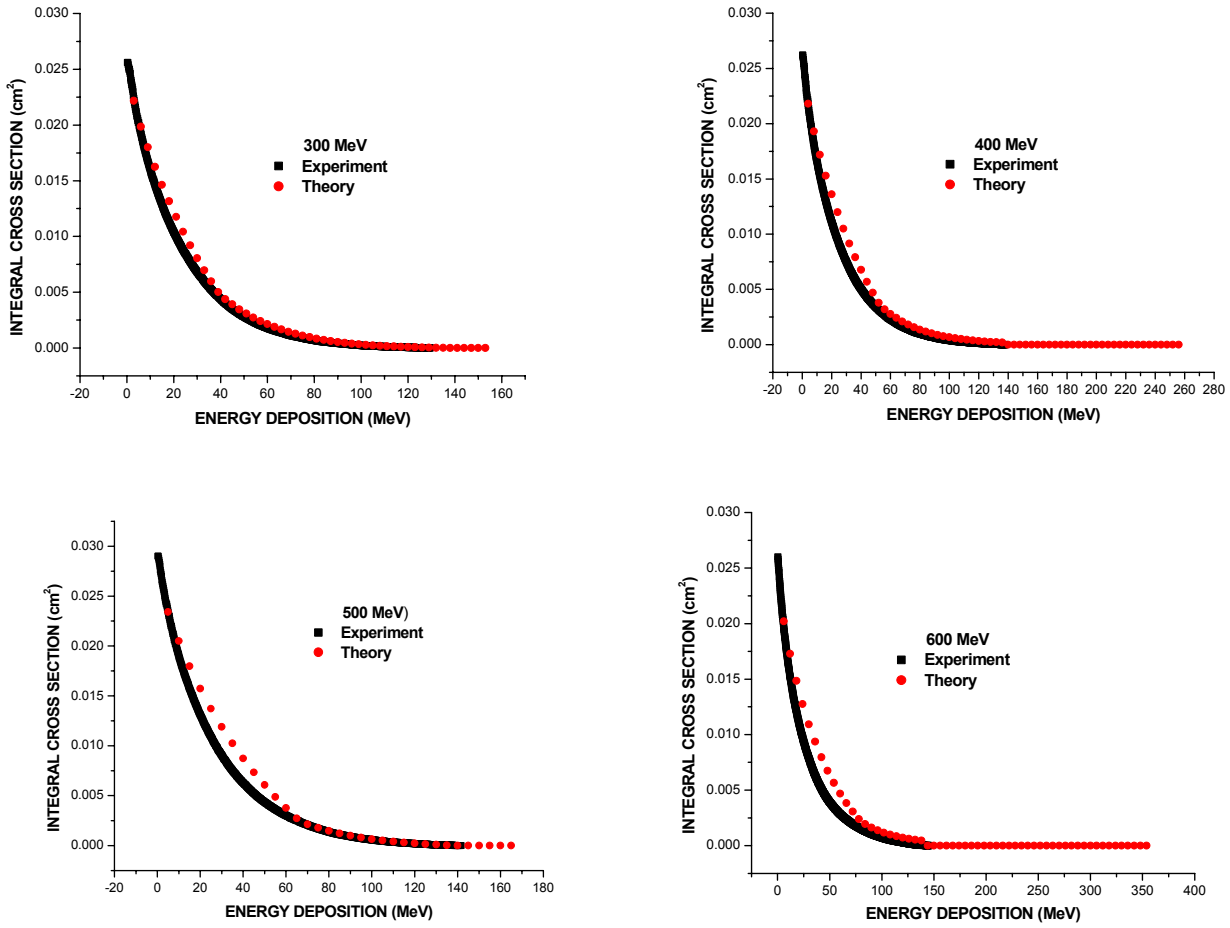

Fig. 14 Number of events in which an energy >E is deposited is plotted versus E the value of the energy deposition. The black data set represents experimental measurements with LANL neutrons and the red set represent theoretical calculations using CUPID with modifications to include contributions from pion production and elastic scattering.

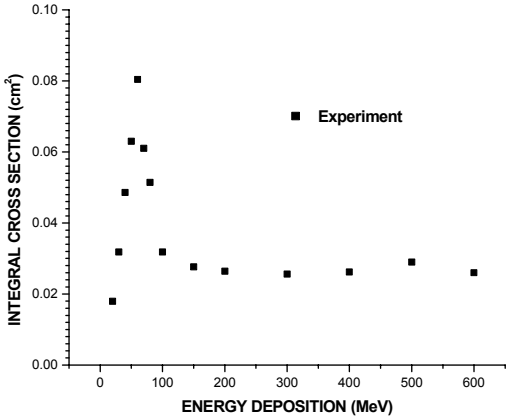

Fig. 15 Experimental total cross section plotted versus the energy of the incident LANL neutron.

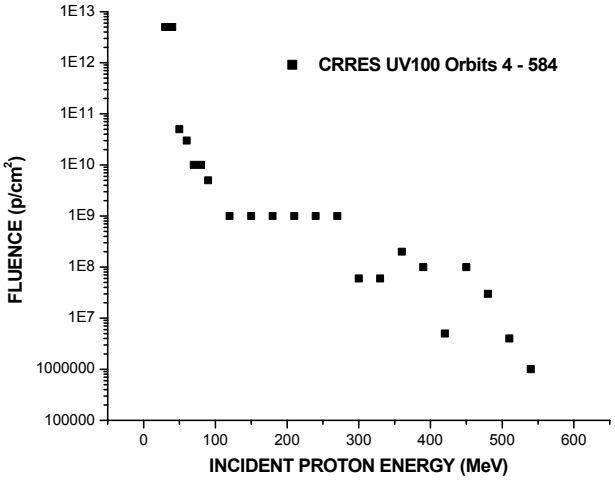

Fig. 16 Fluence of protons incident on the UV100 flown on CRRES for orbits 4 through 584. Data is based on best-fit calculations matching CUPID simulations including corrections for pion production and elastic scattering.

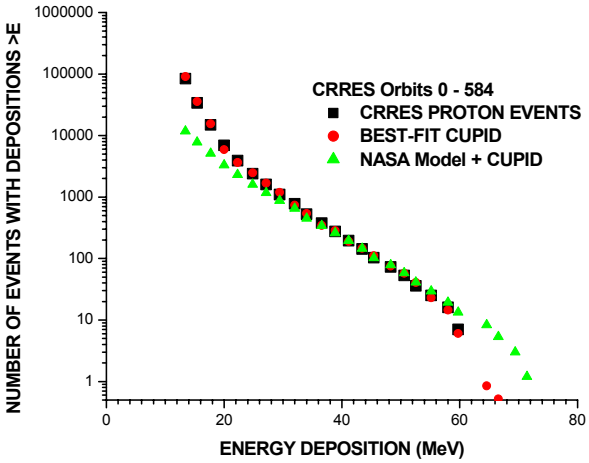

Fig. 17 Comparison of the integral spectrum for the UV100 from orbits 4 through 584 on the CRRES satellite. Black squares are experimental data. The red circles are the spectrum calculated using CUPID corrected for elastic scattering and pion production with the fluence values obtained in this study. The green triangles are the predictions of Reed using the original CUPID and the fluence obtained from the NASA models.

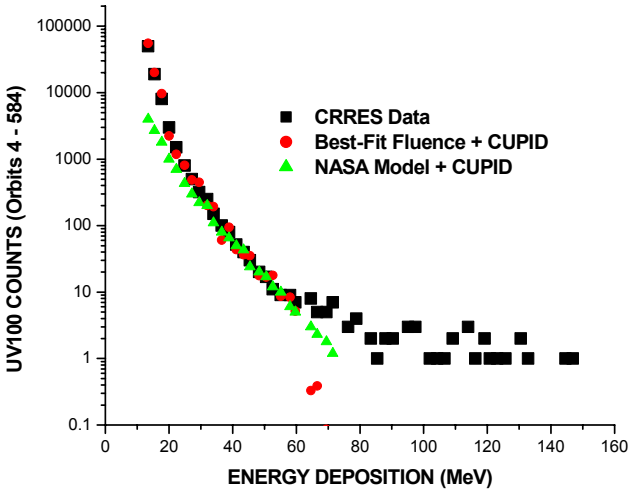

Fig. 18 Differential number of events in which energy E is deposited within the sensitive volume of the UV100 versus E. The black squares represent CRRES measurements during orbits 4 through 584. The red circles represent calculations carried out using CUPID with corrections for elastic scattering and pion production and the best-fit values of the fluence determined above. The green triangles represent earlier predictions of Reed using the original version of CUPID and the fluence values calculated from AP8 model using the USAF B-L coordinates.

APPENDICES

A. "SEU Induced by Elastic Scattering", P.J. McNulty, M.W. Savage, D.R. Roth, and C.C. Foster

B. "Neutron-Induced Pion Production in Silicon-Based Circuits" J.D. Kinnison, R. Maurer, D.R. Roth, P.J. McNulty, and W.G. Abdel-Kader

SEU INDUCED BY ELASTIC SCATTERING

P.J. McNulty[1], M.W. Savage[2], D.R. Roth[3], and C.C. Foster[4]

[1]Dept of Physics and Astronomy, Clemson University, Clemson, SC 29634-1911
[2]Crane Naval Surface Weapons Center, Crane Indiana, 47522
[3]Applied Physics Laboratory, The Johns Hopkins University, Laurel, MD 20723-6099
[4]Cyclotron Facility, Indiana University, Bloomington, IN 47408

ABSTRACT

At low incident nucleon energies elastic scattering events generate more SEUs than spallation reactions in devices with thin sensitive volumes. Reducing the critical charge by lowering the bias increases the incident energy below which elastic scattering dominates SEU production.

I. INTRODUCTION

According to the First Order Model, a memory element upsets when a threshold or critical amount of charge is collected across the sensitive p-n junction. This is equivalent to saying that a critical amount of charge must be generated within the sensitive volume associated with that junction [1]. For this equivalence to be correct requires that the dimensions of the sensitive volume, especially the thickness, be specified correctly. The value of the critical charge depends on the device being tested, its access time, and the operating voltage used during the test. It should, however, be independent of the particle species and incident energy used for the measurements. Previous studies have shown the same SEU parameters fit data obtained with heavy ions and protons [2-5] and protons and neutrons [3]. Other studies show that the dimensions of the sensitive volume can be obtained from either charge collection measurements directly on the devices [1,5] or using Monte-Carlo simulations to determine the optimum dimensions and the value of the critical charge [4].

These successes give us confidence that the First Order Model is a useful approximation, and that the SEU parameters can be determined using these procedures. Moreover, the SEU rates calculated using the parameters determined using these procedures and standard environmental models have given good agreement with rates measured on the CRRES satellite [6,7].

Proton and neutron induced SEU events have previously been successfully modeled assuming that spallation reactions were the dominant mechanism. Spallation reactions were known to generate nuclear recoils that deposited more energy within the sensitive volume than could be obtained from elastic reactions. However, at very low incident energies there are fewer spallation reactions that generate the high-energy recoils. Also, elastic recoils with very low energies have very high values of the linear energy transfer (LET), and if the sensitive volume is very thin, the elastic recoil can deposit more energy than the more energetic (but lower LET) spallation recoil.

We apply our analysis to two SRAMS both of which show an interesting correlation between the SEU cross sections measured with low-energy neutrons emerging from a Pu/Be source and those obtained with high-energy protons. This is illustrated in Fig. 1 where the measured Pu/Be neutron SEU cross sections is plotted for different bias values versus the corresponding cross sections measured with 148 MeV protons. Changing the bias changes the critical charge required to upset the device, and thus changes both the proton and neutron cross section. There are simple power law relationships relating the neutron and proton cross sections for the two devices but they have different slopes, which suggest different mechanisms for upset.

The power-law relationship is not unexpected. Figure 2 shows the results of simulations for protons incident at 20 MeV on sensitive volumes with different dimensions and thresholds for upset plotted versus the corresponding values obtained for 142 MeV protons. All calculations were carried out with the CUPID simulation codes. The relationships clearly depend on the dimensions of the sensitive volume, but the slope does not. We find that these relationships hold for all proton energies and sensitive volumes tried. The object of this analysis is to explain the different slopes observed for the two devices in Fig. 1.

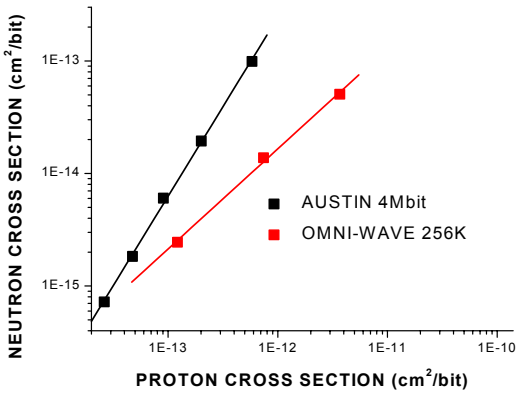

Fig. 1. SEU cross section obtained with Pu/Be neutrons at different bias values plotted versus the corresponding cross section measured with 148 MeV protons.

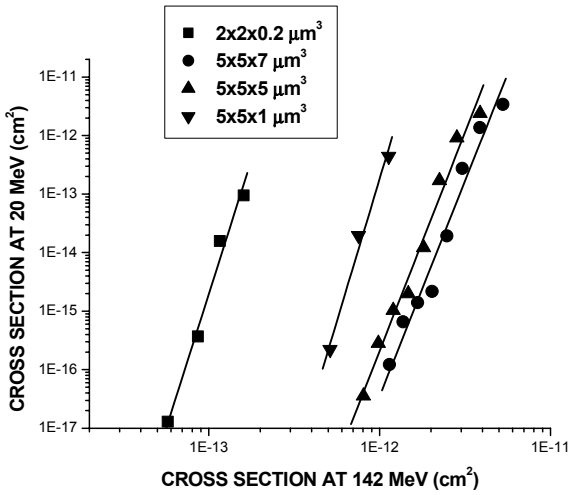

Fig. 2 Cross sections obtained from CUPID simulations for 20 MeV protons incident on a sensitive volume with the dimensions given and various critical charges plotted versus the corresponding cross section obtained with 142 MeV protons.

II. DESCRIPTION OF EXPERIMENT

One of the devices studied was an Austin Semiconductors MCM6246 NMOS SRAM. This device is a repackaged Motorola SRAM, MCM6426. Norman et al. [8] Have also measured proton-induced upsets for a Motorola MCM6246, and the SEU cross sections that group obtained are in agreement with our data. Proton charge-collection measurements as well as reduced-bias single-event-upset measurements were carried at the Indiana Cyclotron Facility. A proton beam of 195.2 MeV incident energy was used, and protons incident at 136.6 MeV and 68.3 MeV were obtained by inserting an appropriate thickness of copper degrader between the device and the undegraded beam. Both the proton charge-collection measurements and the reduced-bias single event upsets were measured under identical conditions. The neutron measurements in this study were obtained at Clemson University using a Pu/Be neutron source. As with the proton studies, both the neutron single event upsets (SEU) and charge-collection measurements were made under identical conditions.

The proton SEU cross sections measured as a function of bias are plotted for different incident proton energies in Fig. 3 for the Austin SRAM. There is a smooth dependence on bias in each case.

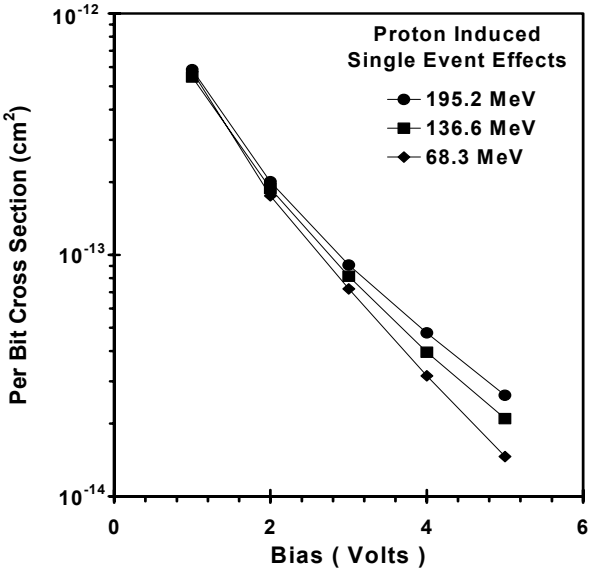

Fig. 3 Cross section versus bias for three different incident proton energies for the Austin MCM.6246 SRAM.

The Pu/Be neutron cross sections measured as a function of bias are plotted in Fig. 4. Again we see a smoothly varying dependence of the SEU cross section with bias indicating an increase of the critical charge and a corresponding decrease in the SEU cross section with bias.

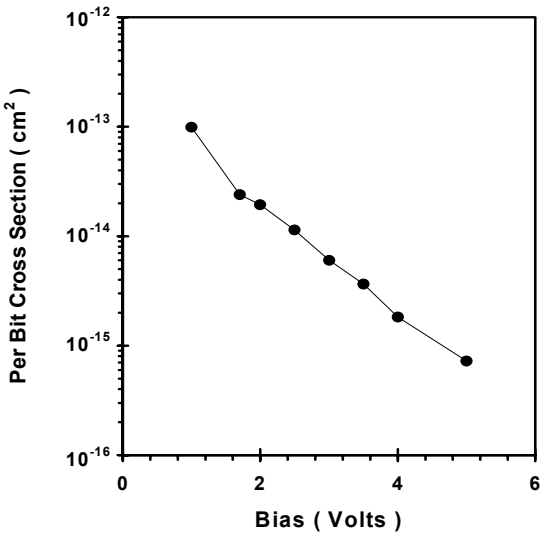

Fig. 4. Cross section versus applied bias for an Austin MCM6246 SRAM exposed to neutrons from a Pu/Be radioactive source at Clemson.

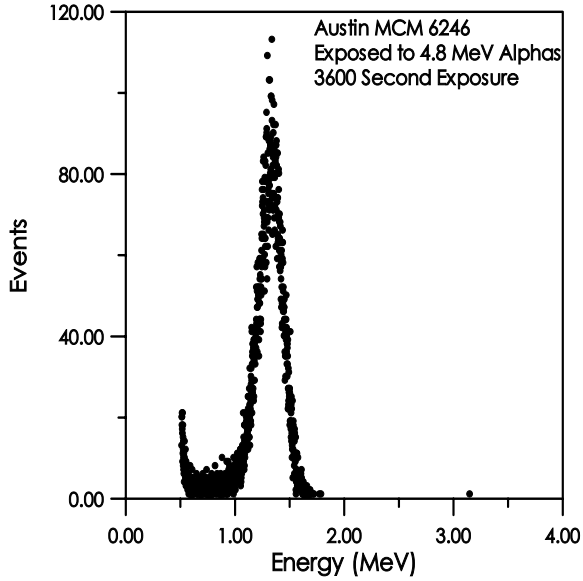

Fig. 5 Charge collection spectrum measured off the power pins of a 4 Mbit SRAM while it is being exposed to alphas from an Americium source.

Traditional charge collection measurements [5] were carried out on the MCM6246 but the data could not be used to determine the dimensions of the sensitive volume. Fig. 5 shows the pulse-height spectrum obtained off the power pins of the device when the device is exposed to alpha particles from an Am/Be source. Normally, the integral number of events under the curve equals the product of the fluence and the total area of the drains. This determines the area and the position of the peak of the spectrum gives the thickness of the sensitive volume [5]. However, this spectrum is narrower than the spectrum normally obtained from an array of drains on an SRAM. The proximity of the particle trajectory to the edge of a drain, typically causes a broader distribution of pulse heights.

It turns out that this NMOS device is in a protective well and the signals in Fig. 4 are actually from the body ties of this large-area well. This explanation is confirmed when the pulse-height spectrum obtained with 195.2 MeV protons is compared in Fig. 6 with the predictions of CUPID for a sensitive volume having the dimensions given by the charge collection measurements assuming a single large area sensitive volume and assuming an array of small-area drains. The data fits well the assumption of a single large-area well.

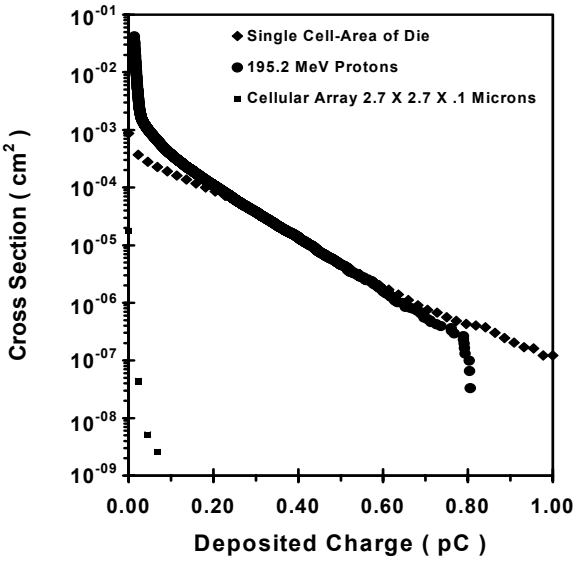

Fig. 6. Comparison of CUPID simulations with the charge-collection spectrum measured off the power pins of the SRAM while the SRAM is exposed to high-energy protons. There is good agreement when the sensitive volume is assumed to be a single volume having the dimensions obtained from the spectrum in Fig. 7, but no agreement with the simulations for an array of sensitive volumes typical of drains.

The alternative method of determining the dimensions of the sensitive volume is described in [2,6], and this method was used in this study. The area occupied by the drains was estimated to be 25% of the

die area, which is in accordance with the normal ratio of drain to total die area that has been observed by this group in the past. The thickness of the sensitive volume was found by taking a succession of CUPID simulations for different values of the thickness and finding the resulting critical charge that best fit each of the SEU cross-sections measured. As the critical charges are independent of the incoming proton energy, the correct thickness of the sensitive volume should be the value which has the lowest standard deviation of the critical charges determined over all proton energies. The plot of the standard deviation in the values of the critical charge determined over the different proton energies at a bias of 5 V are plotted versus the thickness of the sensitive volume in Fig. 7. The minimum is found to be at the smallest values of the thickness, 0.1 μm, corroborating the explanation that the SRAM employ a drain structure to reduce the charge collected at the drain during an ion strike.

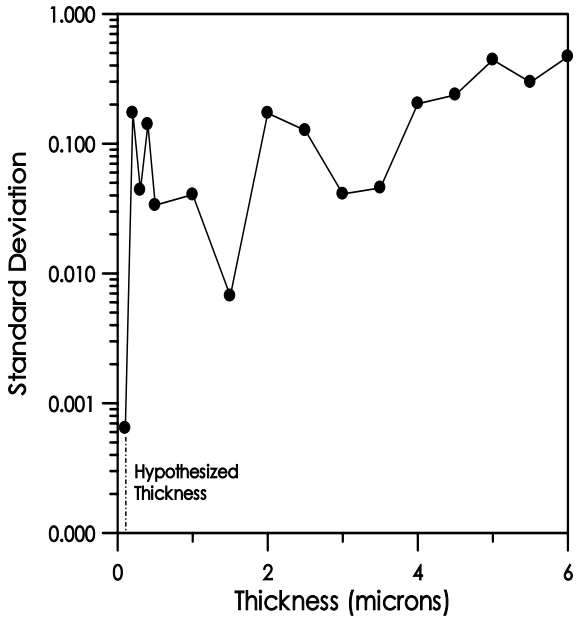

Fig. 7 Standard deviation in the values of the critical charge obtained at different proton energies plotted versus the thickness assumed for the sensitive volume. The optimum value of the thickness is at the minimum of the curve, in this case at the lowest thickness tested, 0.1 μm.

III RESULTS

Using the thickness of 0.1 μm determined from Fig. 7, the charge-collection spectra were calculated by CUPID for all of the incident proton energies. The SEU cross sections measured at each bias and incident energy are listed in Table 1 along with the values obtained with the Pu/Be neutrons. The corresponding values of the critical charges that were obtained from the cross sections and the CUPID simulations are listed in Table 2 and plotted versus bias in Fig. 8.

Table 1
Reduced Bias Proton SEU Experiment.

Per Bit Cross Sections for SEU's at reduced bias in cm^2				
Proton Energy (MeV)	195.2	136.6	68.3	Pu/Be Neutrons
5 Volt Bias	2.62×10^{-14}	2.10×10^{-14}	1.46×10^{-14}	7.23×10^{-16}
4 Volt Bias	4.75×10^{-14}	3.96×10^{-14}	3.16×10^{-14}	1.83×10^{-15}
3 Volt Bias	9.08×10^{-14}	8.16×10^{-14}	7.23×10^{-14}	6.03×10^{-15}
2 Volt Bias	2.01×10^{-13}	1.89×10^{-13}	1.75×10^{-13}	1.94×10^{-14}
1 Volt Bias	5.84×10^{-13}	5.44×10^{-13}	5.75×10^{-13}	

Table 2
Critical Charges in picoCoulombs at Reduced Bias

	195.2 MeV Protons	136.6 MeV Protons	68.3 MeV Protons	Pu/Be Neutrons
5 V Bias	0.0225	0.0226	0.0226	0.0045
4 V Bias	0.0223	0.0224	0.0224	0.0043
3 V Bias	0.0218	0.0219	0.0220	0.0037
2 V Bias	0.0206	0.0208	0.0210	0.0017
1 V Bias	0.0165	0.0170	0.0169	

The CUPID codes were written for use at high incident energies, and as a result, the current versions are not designed for use at low incident energies, neutron or proton. Previous comparisons with 14 MeV neutron spectra obtained with surface-barrier detectors showed that CUPID generated the correct shape of the charge-collection spectrum, but not the correct total number of events. To correct for this, simulations and neutron exposures were carried out for a surface-barrier detector. The flux of incident neutrons necessary to generate the same number of events in the detector was determined and used in the simulations. This should correct for errors in the cross sections used in the codes at these energies and for errors in the strength of the source. These calculations should overestimate the values of the SEU cross section and critical charge. Instead, the critical charge values obtained were lower than the proton estimates.

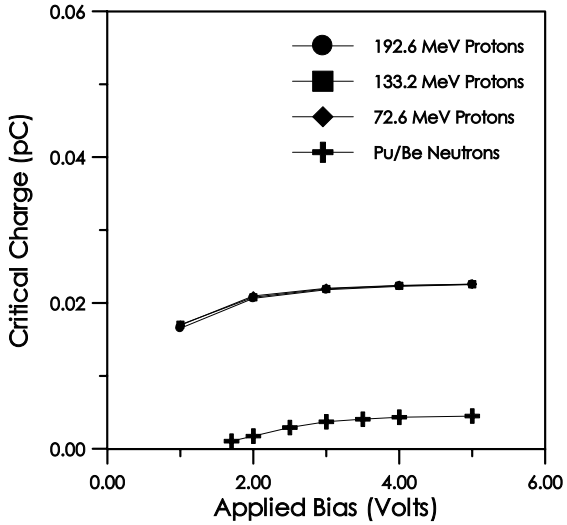

Fig. 8. Critical charges obtained from the measured SEU cross sections and the CUPID simulations plotted versus the value of the bias applied to the device during the measurements.

The values of the critical charge obtained this way are plotted versus applied bias in Fig. 8. The proton-induced critical charge values do not depend on incident proton energy as expected, but the values obtained from the neutron data are much lower than the corresponding proton values. The proton agreement gives us considerable confidence in the values of the dimensions of the sensitive volume used in the simulations. However, the differences between the values of the critical charge obtained with protons and those obtained with neutrons are substantial with the proton values being a factor of four greater than even the overestimated neutron values.

The simplest explanation for the difference between neutrons and protons is the different relative contribution of elastic scattering in the two cases. According to Fig. 8, the value of the critical charge is less than 0.025 pC even at 5 Volts bias. Charge this low can be generated by the recoils from elastic scattering events as well as from the recoil and secondary particles from spallation reactions. Low–energy neutrons generate lower energy recoils in elastic scattering events than do high–energy protons, but many of these recoils will have higher values of LET and sufficient range that they can generate more than a critical amount of charge within the 0.1 μm layer of the sensitive volume. The relative contribution of these elastic recoils should be greater for the low-energy neutrons than for the high-energy protons. This would lead to a lower apparent value of the critical charge if comparison were made to models that only include contributions from spallation reactions.

In order to analyze this disagreement further, the results for our 4 Mbit SRAM are compared with data obtained from a 256K SRAM from Omni-Wave analyzed previously in [3]. The 256K SRAM gave agreement between the values of the critical charge obtained with low-energy neutrons and high-energy protons. The measured per bit SEU cross sections for both devices are plotted versus bias in Fig. 9. The curves for the two devices are parallel, and are reasonable agreement at all bias values.

Fig. 9. SEU per-bit cross section for two device plotted

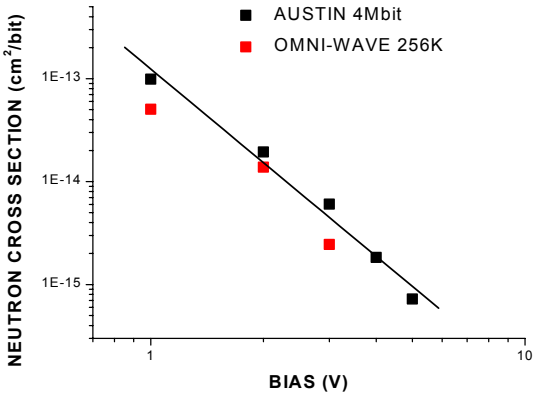

versus the bias applied during the exposure.

When we plot the measured SEU cross sections obtained with energetic protons, we see something quite different. In this case, the 256 K SRAM has higher cross sections at all energies, and there is a dramatic increase in the cross sections as the bias is reducedscatter. The proton SEU cross sections for the two devices are in reasonable agreement at high bias values, but there is a sharp increase at low bias values but only for the 256K device. We attribute this to the onset of elastic scattering interactions that dominate at low energy depositions. To illustrate how elastic interactions can dominate for very low incident energies, but not contribute significantly at high proton energies comparisons of the measured SEU cross sections are compared with calculations in Figs. 11 and 12 for the 4 Mbit device. There is no evidence for a significant contribution from eleastic scattering for biases above 1 V. For the low-energy neutrons, the measured cross sections are consistent with elastic scattering being the dominant mechanism.

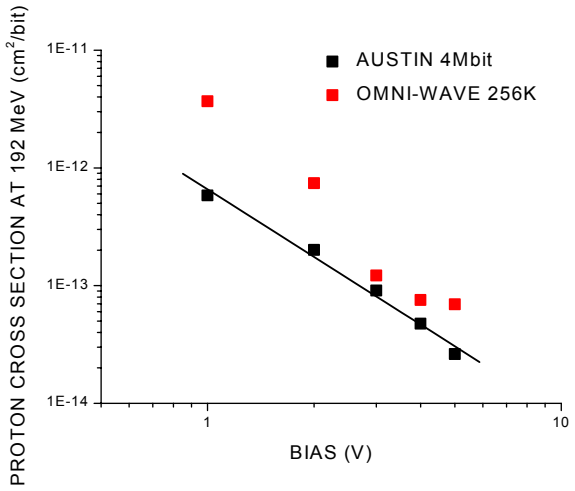

Fig. 10. SEU cross section measured at 192 MeV versus bias.

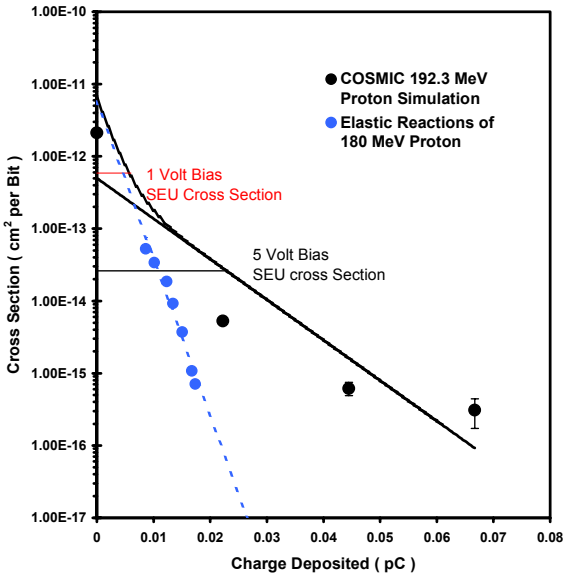

Fig. 11 SEU cross section versus the value of the critical charge for elastic scattering (dotted curve) and spallation reactions (solid curve).

IV. SUMMARY AND CONCLUSIONS

Evidence of a significant discrepancy between the proton induced SEU response and the response to neutrons of the Austin MCM6246, a 4 Mbit SRAM was explained in terms of elastic scattering SEU events not taken into account by the model. The SEU cross-sections measured with low-energy neutrons from a Pu/Be radioactive source were much higher than would be expected from predictions based on the measured proton SEU cross-sections. Both the proton and neutron data showed a small decrease in the critical charge with applied bias, but in both cases this small change led to large increases in SEU rates clearly demonstrating the value of operating the SRAM at the higher bias values to lower the SEU sensitivity.

This part has a feature that prevents the user from obtaining useful information on the dimensions of the sensitive volume by analysis of the charge-collection spectrum. The charge-collection spectrum obtained with Am/Be alphas was consistent with collection from a single p-n junction with the size of the entire die. This may be the result of some well-like structures introduced to reduce the contributions to the drain current from cosmic-ray transients.

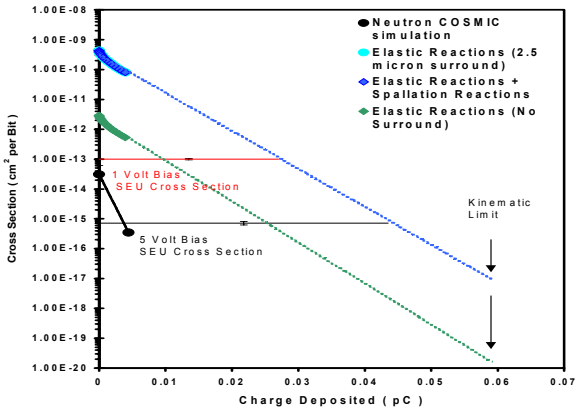

Fig. 12. Cross section for SEU events versus the value of the critical charge for low-energy neutrons with a spectrum typical of a Pu/Be source.

REFERENCES

1. P.J. McNulty, "Predicting Single Event Phenomena" in Microelectronics for the Natural Radiation Environments of Space, P.J. McNulty Ed. (IEEE Short Course, 1990) pp 3-1 to 3-93.
2. W.J. Beauvais, P.J. McNulty, W.G. Abdel Kader, R.A. Reed, "SEU Parameters and Proton-Induced Upsets," RADECS 93,540-545 (1993)
3. M.W. Savage, P.J. McNulty, D.R. Roth, C.C. Foster, "Possible Role for Secondary Particles in Proton-Induced Single Event Upsets of Modern Devices," IEEE Trans. Nucl. Sci. , 45, 2745-2751 (1998)
4. P.J. McNulty, W.J. Beauvais, D.R. Roth, "Determination of SEU Parameters of NMOS and CMOS SRAMS," IEEE Trans. Nucl. Sci. 38, 1463-1470 (1991).
5. R.A. Reed, P.J. McNulty, W.J. Beauvais, "Charge Collection Spectroscopy," IEEE Trans. Nucl. Sci., 40, 1876-1884 (1993).
6. R.A. Reed, P.J. McNulty, W.J. Beauvais, W.G. Abdel-Kader, E.G. Stassinopoulos, J.C.L. Barth, "A Simple Algorithm for Predicting Proton SEU Rates in Space Compared to The Rates Measured on the CRES Satellite," IEEE Trans. Nucl. Sci., 41, 2389-2395 (1994)
7. P.J. McNulty et al., Int. J. Radiat. Instrum., Part D, Nucl. Tracks and Radiat. Meas., 19, 929-938 (1991).
8. E. Normand, "Extension of the Burst Generation Rate Method for Wider Application to Proton/Neutron – Induced Single Event Effects," IEEE Trans. Nucl. Sci.,45, 2904-2914 (1998)
9. P.J. McNulty, Ph. Roche, J.M. Palau, and J. Gasiot, IEEE Trans. This issue.
10. E.L. Peterson, "The SEU Figure of Merit and Proton Upset Rate Calculations," IEEE Trans. Nucl. Sci.,45, 2550-2561 (1998)

Neutron-Induced Pion Production in Silicon-Based Circuits

J.D. Kinnison, R. Maurer, D.R. Roth , P.J. McNulty, and W.G. Abdel-Kader

Abstract – We compare deposition spectra from mono-energetic neutron irradiation to CUPID simulations of the same neutron exposures. CUPID does not agree with the experimental data unless pion production is included in the neutron-nucleon interaction. Pion-production events result in slightly more SEE events for devices with relatively large sensitive volumes and low thresholds for upset but dramatically fewer events for the same sensitive volume when the threshold is high.

I. INTRODUCTION

Protons in the trapped radiation belts have kinetic energies that extend up to hundreds of MeV with the proton flux decreasing sharply with increasing incident energy. Neutrons generated by cosmic rays in the upper atmosphere or in the skin or shielding of spacecraft or aircraft also extend to energies well above the threshold for production of pions. [1] Pions have rest masses about 140 MeV, and interact strongly with the nucleons in the atomic nuclei. If a pion is created within a heavy nucleus and immediately absorbed, the rest mass of about 140 MeV would be available for the continued breakup of the target nucleus and eventually result in a dramatic increase in the localized energy deposition. However, if the pion escapes from the target nucleus with momentum **p**, that momentum of the target nucleus and the resulting localized energy deposition will also be increased but by a much smaller amount.

In order to produce pions, energy at least equal to the rest mass of the pion must be available in the center of momentum (CM) frame. [2,3] The fundamental interaction is between a high energy proton or neutron and a nucleon within a silicon nucleus. Note that in this CM interaction both the incident particle and the target nucleon have kinetic energy. In the lab frame, the incident particle energy needed to create a pion is approximately twice the rest mass of the pion. If the nucleon is directed toward the incident particle in the interaction, the momentum of the nucleon contributes to the energy from which the pion is created. As a result, pion production begins for incident particle energy well below the pion threshold in the lab frame. Figure 1 shows the onset of pion generation in the efficiency of the silicon detector described below as a function of neutron energy. Note that this curve shows an increase in efficiency (and correspondingly, interaction cross-section) above about 250 MeV which represents the generation of a single pion, and an additional increase above about 500 MeV where two-pion processes begin to occur.

At energies below 1000 MeV, pions are only going to be produced in the most energetic (head on) collisions between the incident neutron and target nucleons. It is important to note that these collisions would have resulted in spallation reactions anyway, and these spallation events would have resulted in very large localized energy depositions. If the pion leaves the sensitive volume without further nuclear interactions, the localized energy deposition may be reduced from what would have resulted from the same collision minus pion production. Since Si is a light nucleus, most of the nucleons inside the nucleus are on the surface where any pions generated would be likely to escape without being absorbed. Since these pions have no LET if neutral and very low LET if charged, the localized energy deposition can be considerably less if a head-on collision results in a pion being produced than if no pion was produced.

In this work, we compare energy deposition spectra from mono-energetic n-Si reactions in a thick silicon detector to simulation of the experiments using CUPID [4]. Energy deposition models such as CUPID based on the physics of individual interactions in a silicon volume are used to predict single event effects rates in microelectronics. This comparison was used to investigate the fidelity of CUPID for energetic interactions, and as discrepancies were found, to develop an improved version of CUPID that more accurately simulates depositions from high energy interactions that include pion production.

II. EXPERIMENT

In August 2000, we measured energy depositions in a 5 mm lithium-drifted silicon detector from neutrons with energy ranging from 20 to 800 MeV at the Los Alamos Neutron Science Center using the 90 m beam line of the Weapons Neutron Research (WNR) facility. This beam is a mixed spectrum of neutron energies produced by spallations from a high energy proton beam impinging on a tungsten target. [5]

Pulse heights for each neutron interaction in the silicon detector were measured and recorded. In addition, our detector was integrated into the neutron time-of-flight spectrometer on the 90 m beam line, and the energy of the

Manuscript received 22 July, 2003. This work was supported in part by the National Aeronautics and Space Administration under NASA Cooperative Agreement 9-58 with the National Space Biomedical Research Institute and NASA under Research Grant NAG8-1695 with the Marshall Space Flight Center.

J. D. Kinnison is with the Applied Physics Laboratory, Johns Hopkins University, 11100 Johns Hopkins Road, Laurel, Maryland, 20723-6099 (email: jim.kinnison@jhuapl.edu) and with Clemson University, Clemson, South Carolina, 29117.

R. H. Maurer, and D. R. Roth are with the Applied Physics Laboratory, Johns Hopkins University, 11100 Johns Hopkins Road, Laurel, Maryland, 20723-6099.

P. J. McNulty is with the Department of Physics, Clemson University, Clemson, South Carolina, 29634-0978.

W. Abdel-Kader is with South Carolina State University, Orangeburg, South Carolina, 29117.

incident neutron for each pulse in the silicon detector was simultaneously recorded. This data gave energy deposition spectra for each time-of-flight bin. These bins are narrow (~1 MeV), and so each bin represents a nearly mono-energetic neutron "beam", each of which is associated with an energy deposition spectrum in the silicon detector for that neutron energy bin. Further description of these measurements may be found in [6].

The detector used in this study is a 2 cm^2 by 5 mm lithium-drifted silicon device manufactured by Ortec. The resolution of the detector is less than 1%, and the pulse height electronics were designed to measure deposited energy from 2 to 250 MeV. A sodium iodide scintillator was used as a charged particle veto to ensure that only neutron events were counted. In addition, a uranium fission foil detector was used with the time-of-flight spectrometer to provide a simultaneous monitor of the neutron energy spectrum from the WNR beam. [7]

III. CUPID Model

Standard CUPID Model

The CUPID code is a cascade-evaporation of nucleon-nucleus interactions for silicon. Nuclei are modeled in CUPID as a gas of energetic nucleons through which an incident particle may pass. Nucleons are assigned energy and momentum within the nucleus, and this momentum can significantly contribute to the total energy deposited in the silicon volume. Interactions take place initially when an incident particle strikes a nucleon, which in turn may strike others. This results in a cascade of particles in the nucleus that ends when one or more are emitted from the nucleus, which is left in an excited state. In the second stage of the interaction - the evaporation stage – the nucleus is modeled as a Fermi gas confined in a potential well. A few nucleons with the correct energy and momentum can escape the well, reducing the overall energy of the nucleus. The end result of the evaporation phase is a residual nucleus with its kinetic energy and momentum determined by the emitted particles.

Several different energy mechanisms are modeled in CUPID: i) ionization of the target material if the incident particle is charged; ii) ionization by cascade and evaporation particles, and iii) ionization by the residual nucleus. CUPID models the target as a finite volume, and so effects such as particle escapes from the active region are included. The result of a CUPID calculation is the interaction cross-section as a function of deposited energy, which is essentially the frequency distribution of energy depositions normalized by the area of the interaction volume. Large energy depositions are seen in those cases where the incident particle and an interacting cascade nucleon hit head on. Standard CUPID does not include mechanisms to account for elastic scattering of the silicon nucleus by the incident particle, nor does it include the generation of pions in nuclear reactions where the energy is greater than the threshold for pion reactions to take place.

Pion Modification to CUPID

Pions are generated in nucleon-nucleon reactions when more than the pion rest mass energy is available in the center of mass frame of the interaction. When incident on a stationary nucleon, a proton or neutron with more than approximately 280 MeV in the lab frame meets this criterion. However, CUPID models nuclei with moving constituents, and the momentum of the nucleon can contribute to the lab frame interaction. The result is that pion generation can occur when the incident proton or neutron energy is well below 280 MeV. Those events in the standard CUPID model for which large energy depositions are calculated are exactly those events that in reality would produce pions. Since pions are low LET particles, they do not significantly contribute to the deposition of energy in the target. Therefore, when pions can be produced in a large volume such as the 5 mm detector, CUPID should under-predict the number of low energy depositions and over-predict the number of large energy depositions. This behavior is found in our results as discussed below.

We propose a simple modification to CUPID to model the production of pions in p- or n-Si reactions. Assume that all high energy deposition events should have been pion-producing events, that pions are generated with low kinetic energy, and that pions leave the active volume without depositing energy. For each event with deposited energy greater than 141 MeV (the rest mass of the pion plus a small kinetic energy) calculated by CUPID, subtract 141 MeV. If the deposited energy is still greater than 141 MeV, subtract an additional 141 MeV, representing the generation of a second pion. CUPID was modified to perform this subtraction automatically on an event-by-event basis as it calculates interaction cross-section curves, and this modified form of CUPID was used to generate all the curves labeled "Pion Model" in subsequent figures.

IV. Results

Figures 2 – 7 compare the experimental neutron data with CUPID and modified CUPID calculations for incident neutrons in a volume representative of the 5 mm detector for incident energies from 200 MeV to 600 MeV. For each incident neutron energy, both integral and differential cross-sections are given. Note that neither CUPID nor the modified CUPID includes energy depositions from elastic n-Si reactions, which are non-nuclear interactions. Figures 2-7 show discrepancies at very low energy deposition for all neutron energies between the experimental data and the CUPID calculations; the discrepancy is due to the presence of elastic interactions that are not modeled.

Below Pion Threshold

For energies below about 280 MeV, pion-producing events are not expected to significantly contribute to the energy deposition spectrum in the detector. In this region, the CUPID and the modified CUPID simulations match the experimental data to less than 0.1%. As the energy increases to 200 MeV, the disagreement between CUPID and the experimental data increases at high energy depositions while

still remaining small compared to the total cross-section. As described above, rare head-on collisions between the incident particles and nucleons in the silicon nucleus may be energetic enough to allow pion generation. This accounts for the observed discrepancy at energies lower than the threshold of 280 MeV.

Above Pion Threshold

As the incident neutron energy is increased, the discrepancy between the experimental data and CUPID simulations continues to increase. As expected from the efficiency curve presented in Figure 1, pion-generating processes become more and more important as this energy increases. The modified CUPID simulations, however, agree with the experimental data to a remarkable degree given the simplicity of the modifications to the CUPID model. The only remaining discrepancy between the experiment and the modified CUPID model is in the elastic collision mechanism, which is not modeled.

Figure 8 presents the maximum deposition for the experimental data, the standard CUPID model and the pion modification to CUPID. Clearly the pion modification more closely describes the experimental data.

V. Discussion

This is the first comparison of theory and experiment for neutron-induced energy deposition in large sensitive volumes. The volume of this detector is much larger than the sensitive volumes associated with the logic cells of modern microelectronics. However, it is comparable to the sensitive volumes of the larger structures used in Si-based photonics which are very sensitive to single event effects. At least up to the incident neutron energies below the threshold for pion production (50 MeV - 200 MeV), CUPID gives a very reasonable fit to the energy deposition spectra over the entire range of energy depositions. Above the threshold, the disagreement with CUPID is primarily at very large energy depositions where pion production appears to dominate. The principal effect of pion production is to remove the highest events, and even at energies as high as 600 MeV, this is less than 10% of the total number of spallation events.

For sensitive large volume devices, the effect of the pion modification is quite small. The main effect is a shift of large energy events to lower depositions via energy loss in the pion escape. However, for less sensitive devices, standard CUPID will over-predict the number of large deposition events in a high energy proton or neuron environment, and will correspondingly over-predict the device cross-section. In fact, for some devices, CUPID may predict events when none are possible in actuality.

Some photonic devices use materials with higher atomic weight than silicon. In these devices, the target nucleon may be deeper in the nucleus than in silicon, and the pion may be more likely to be absorbed before emerging. Interactions due to absorption would result in higher deposition events, and the modifications to CUPID presented here would not adequately represent the physics of the interaction. Additional modifications to CUPID would be necessary to include the possibility of pion absorption in the nucleus. Standard CUPID is likely to over-predict the cross-section in this cases, but not to such a large degree as for lighter materials such as silicon.

For modern microelectronics with much smaller sensitive volumes than used here, the situation is also different. On the one hand, pion interactions reduce the total energy available for deposition in the sensitive volume. However, these events are dominated at large energy depositions by the contribution of the nuclear recoil. Conservation of momentum implies that the recoiling nucleus has a contribution from the emerging pion, and that contribution is larger in pion interactions than would result from protons and neutrons emerging from a head-on event in different directions. From these two effects, it is not clear whether standard CUPID would under- or over-predict device cross-sections. It is likely that for sensitive devices (i.e., those susceptible to proton upset), other effects dominate and standard CUPID models cross-sections well. For less sensitive devices, CUPID may underestimate the cross-section due to the increased recoil energy when pions are considered. Further work needs to be done to understand the fidelity of the CUPID model when pions are neglected.

VI. References

[1] J. Barth, "Modeling Space Radiation Environments," Short Course presented at the 1997 IEEE Nuclear and Space Radiation Effects Conference, Snowmass Village, Colorado, 21 July, 1997.

[2] E. Segre, *Nuclei and Particles: an Introduction to Nuclear and Subnuclear Physics*, 2nd Edition, W. A. Benjamin, New York, 1965

[3] W. E. Burcham, *Nuclear Physics: an Introduction*, Longman Group Limited, London, 1963.

[4] G. Farrell, *Energy Deposition by Nuclear Interactions in Microscopic Volumes*, PhD Thesis, Clarkson University, May 1983.

[5] P. W. Lisowski, C. D. Bowman, G. J. Russell and S. A. Wender, "The Los Alamos National Laboratory Spallation Neutron Sources," *Nucl. Sci. Eng*., **106**, 208 (1990).

[6] J. D. Kinnison, R. H. Maurer, D. R. Roth and R. C. Haight, "High-Energy Neutron Spectroscopy with Thick Silicon Detectors," *Rad. Res*., **159**, 154-160 (2003).

[7] S. Wender, S. Balestrini A. Brown, R. C. Haight, C. M. Laymon, T. M. Lee, P. W. Lisowski, W. Mc Corkle, R. O. Nelson and N. W. Hill, "A Fission Ionization Detector for Neutron Flux Measurements at a Spallation Source," *Nucl. Instrum. Methods Phys. Res.,* **A 3 3 6**, 226 (1993).

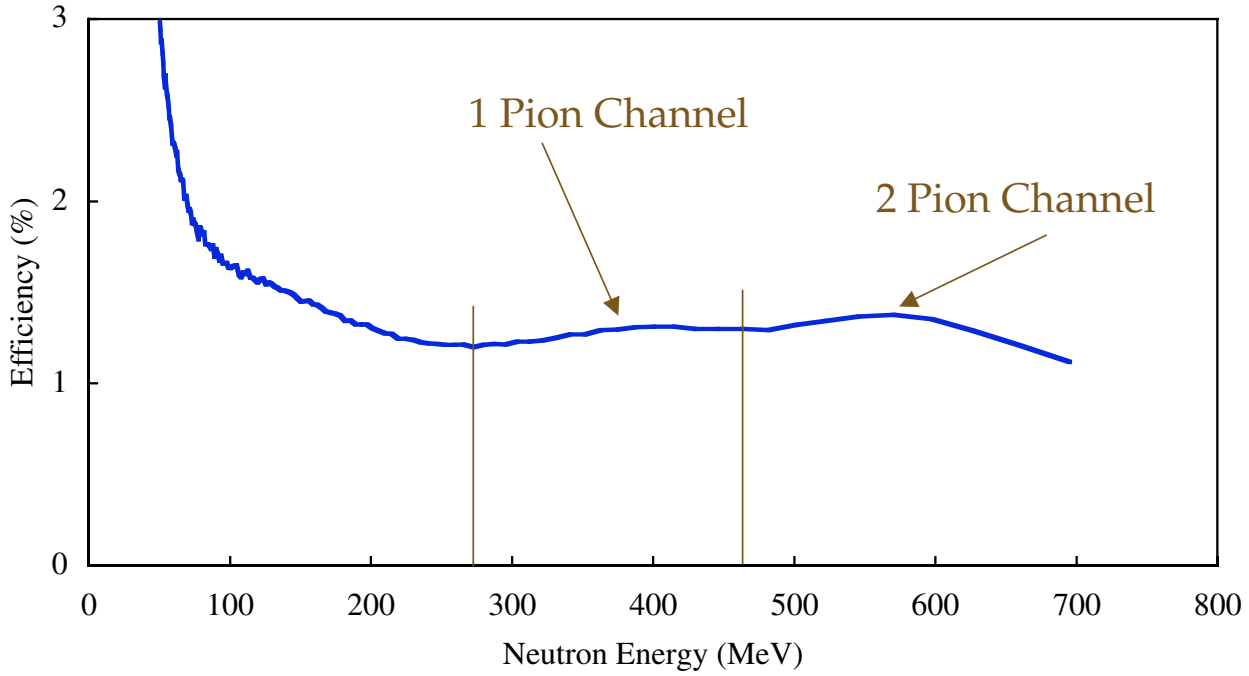

Figure 1. Efficiency of a thick silicon detector for detecting neutrons as a function of incident particle energy. The peaks indicated show the onset of interactions that generate one or two pions.

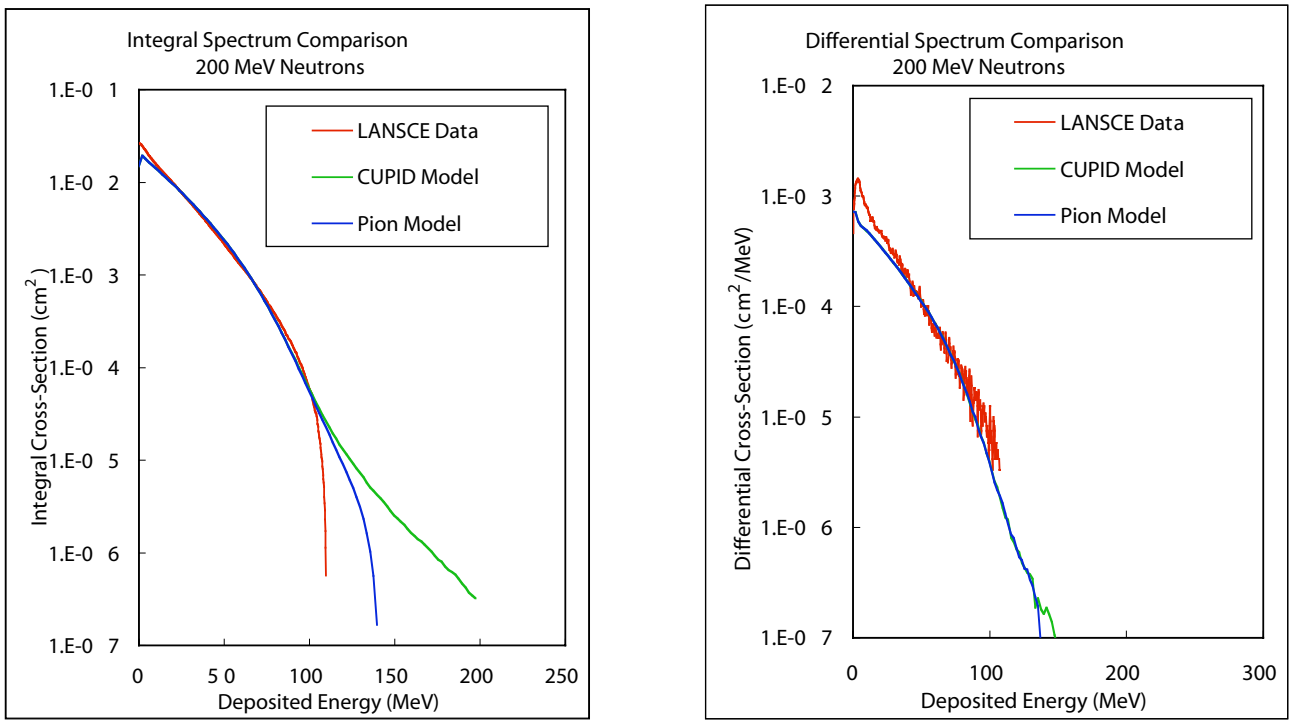

Figure 2. Comparison of a) integral and b) differential energy deposition spectra for 200 MeV incident neutrons.

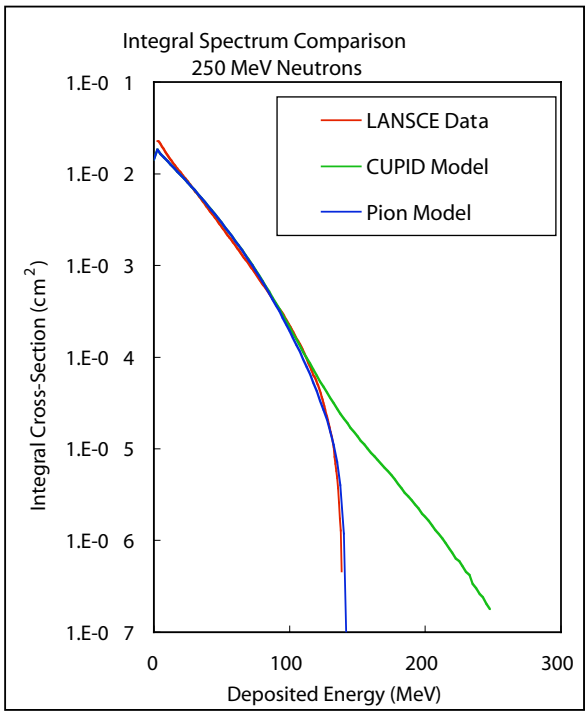

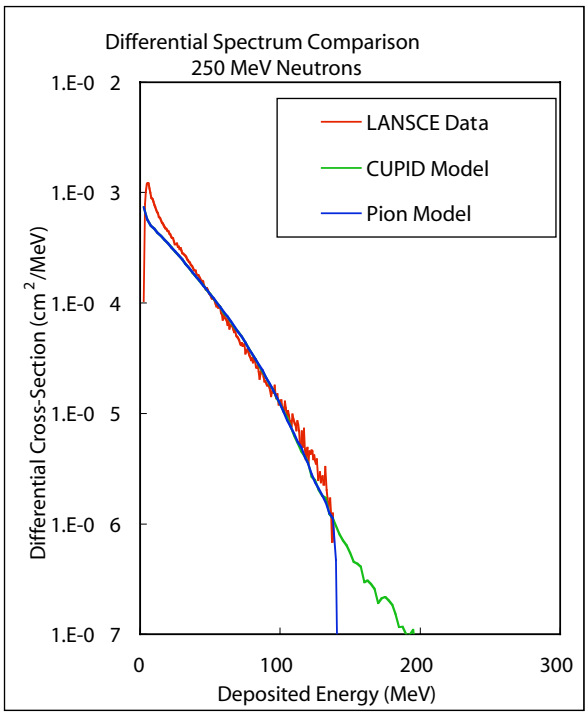

Figure 3. Comparison of a) integral and b) differential energy deposition spectra for 250 MeV incident neutrons.

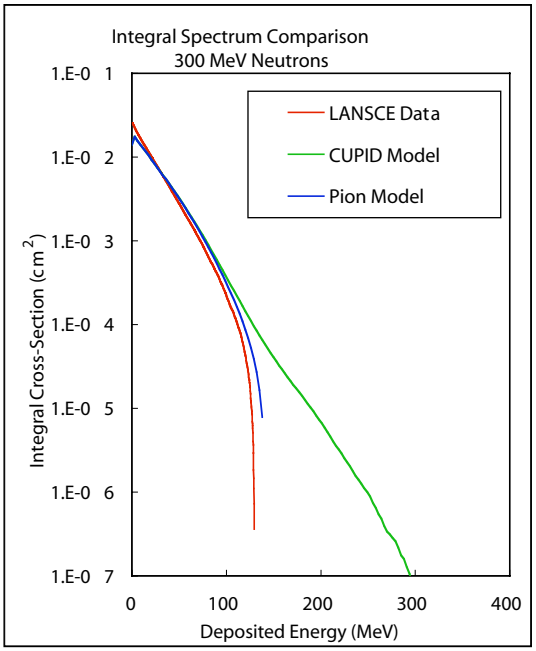

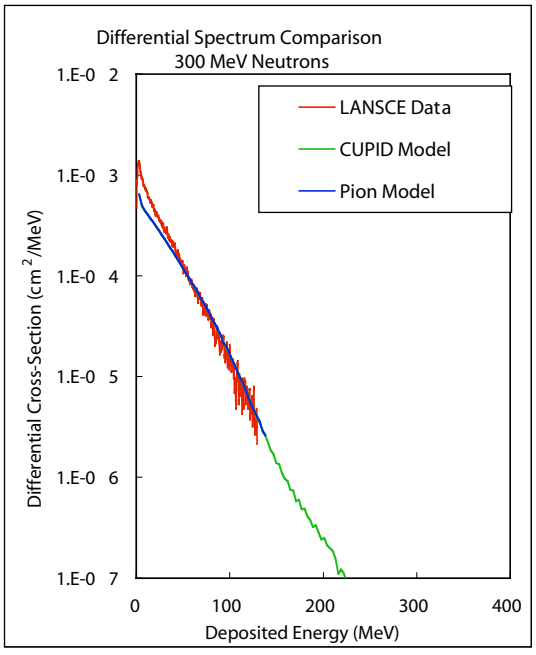

Figure 4. Comparison of a) integral and b) differential energy deposition spectra for 300 MeV incident neutrons.

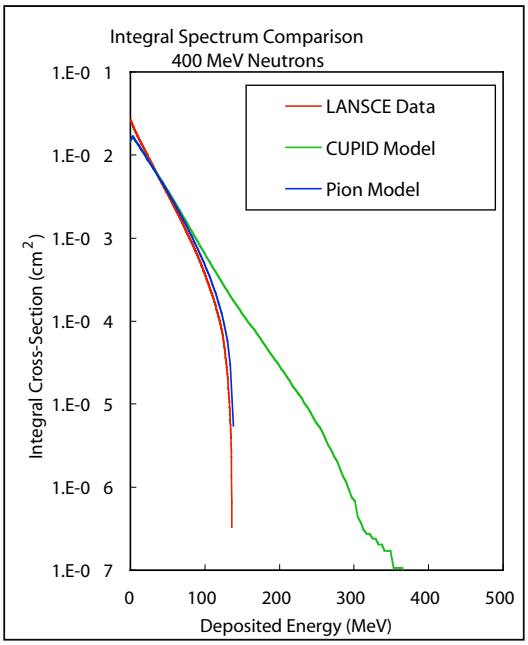

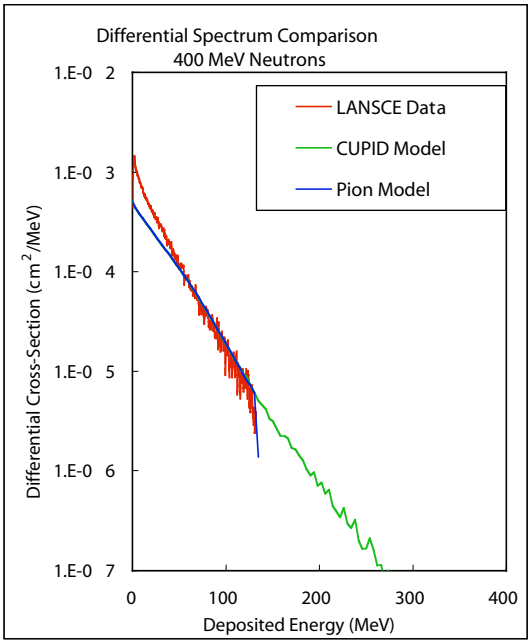

Figure 5. Comparison of a) integral and b) differential energy deposition spectra for 400 MeV incident neutrons.

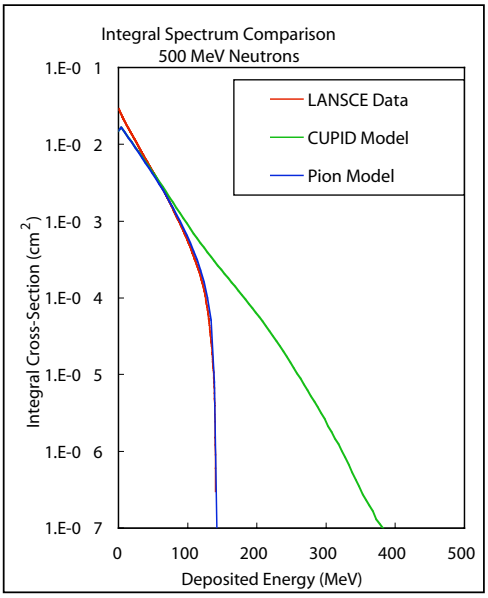

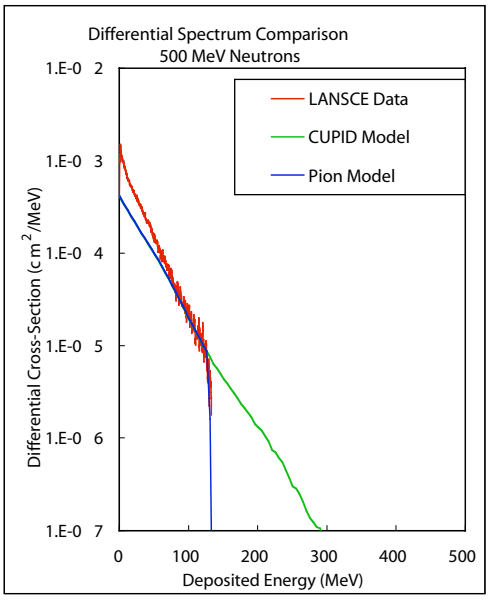

Figure 6. Comparison of a) integral and b) differential energy deposition spectra for 500 MeV incident neutrons.

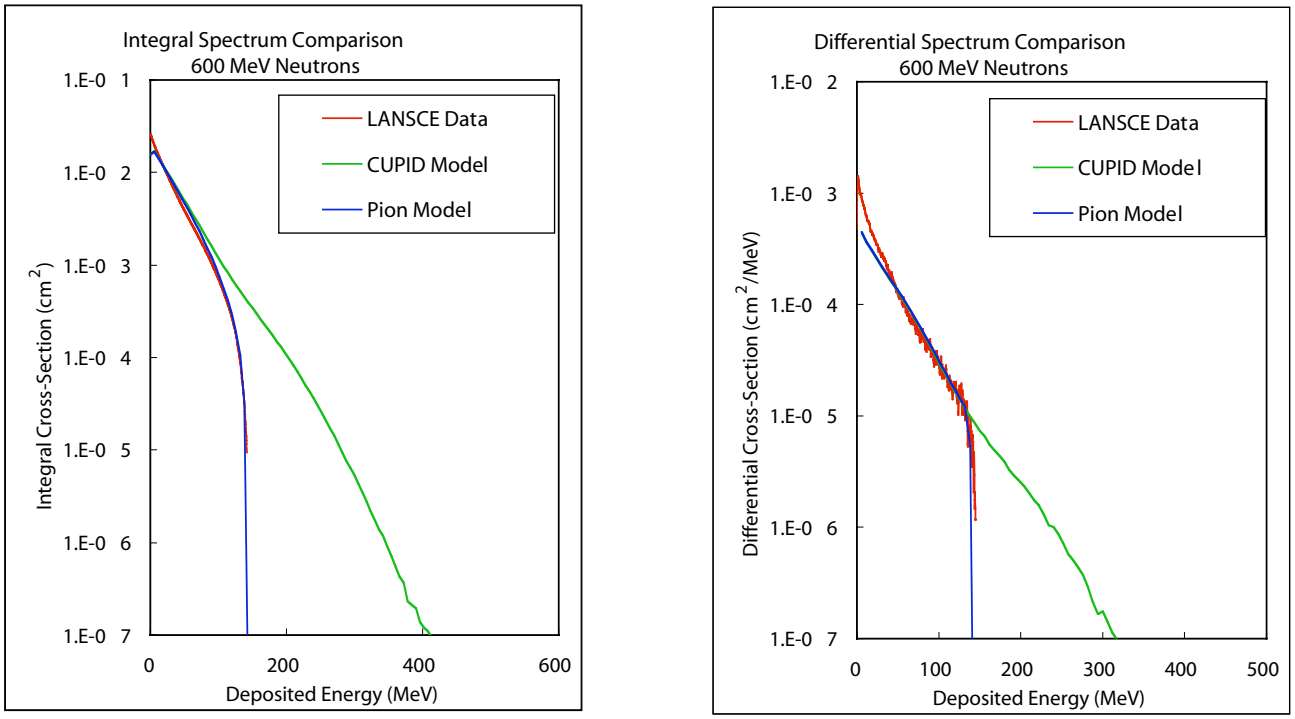

Figure 7. Comparison of a) integral and b) differential energy deposition spectra for 600 MeV incident neutrons.

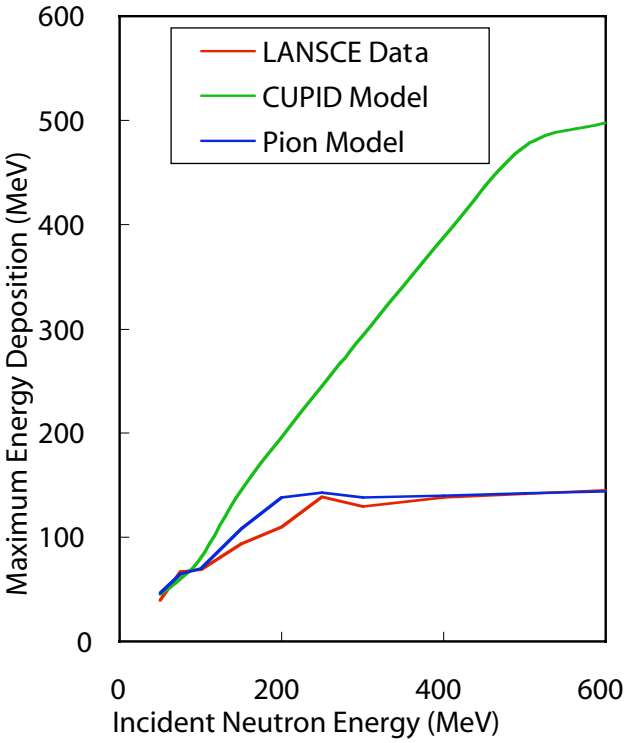

Figure 8. Comparison of maximum deposition energies for experimental data, the standard CUPID model and the modified CUPID model as a function of incident neutron energy.

REPORT DOCUMENTATION PAGE

Form Approved
OMB No. 0704-0188

1. AGENCY USE ONLY *(Leave Blank)*	2. REPORT DATE	3. REPORT TYPE AND DATES COVERED
	June 2004	Contractor Report

4. TITLE AND SUBTITLE

Analysis of CRRES PHA Data for Low-Energy-Deposition Events

5. FUNDING NUMBERS

H–32495D

6. AUTHORS

P.J. McNulty

7. PERFORMING ORGANIZATION NAMES(S) AND ADDRESS(ES)

Clemson University
118 Kinard Laboratory
Clemson, SC 29634

8. PERFORMING ORGANIZATION REPORT NUMBER

M–1110

9. SPONSORING/MONITORING AGENCY NAME(S) AND ADDRESS(ES)

NASA's Space Environments and Effects (SEE) Program
George C. Marshall Space Flight Center
Marshall Space Flight Center, AL 35812

10. SPONSORING/MONITORING AGENCY REPORT NUMBER

NASA/CR—2004–213227

11. SUPPLEMENTARY NOTES

Prepared for NASA's Space Environments and Effects (SEE) Program by Clemson University
Technical Monitor: Donna Hardage, NASA Marshall Space Flight Center

12a. DISTRIBUTION/AVAILABILITY STATEMENT

Unclassified-Unlimited
Subject Category 93
Availability: NASA CASI (301) 621–0390

12b. DISTRIBUTION CODE

13. ABSTRACT *(Maximum 200 words)*

This effort analyzed the low-energy deposition Pulse Height Analyzer (PHA) data from the Combined Release and Radiation Effects Satellite (CRRES). The high-energy deposition data had been previously analyzed and shown to be in agreement with spallation reactions predicted by the Clemson University Proton Interactions in Devices (CUPID) simulation model and existing environmental and orbit positioning models (AP-8 with USAF B-L coordinates). The scope of this project was to develop and improve the CUPID model by increasing its range to lower incident particle energies, and to expand the modeling to include contributions from elastic interactions. Before making changes, it was necessary to identify experimental data suitable for benchmarking the codes; then, the models to the CRRES PHA data could be applied. It was also planned to test the model against available low-energy proton or neutron SEU data obtained with mono-energetic beams.

14. SUBJECT TERMS

CRRES, PHA, low-energy deposition, SEU, CUPID, pion, elastic scattering

15. NUMBER OF PAGES

40

16. PRICE CODE

17. SECURITY CLASSIFICATION OF REPORT	18. SECURITY CLASSIFICATION OF THIS PAGE	19. SECURITY CLASSIFICATION OF ABSTRACT	20. LIMITATION OF ABSTRACT
Unclassified	Unclassified	Unclassified	Unlimited